https://doi.org/10.5194/egusphere-2026-5374
Preprint. Discussion started: 16 September 2026

Global fuel and burned area reconstructions and projections for 1950–2100

Joe McNorton[1], Edward Comyn-Platt[1], Francesca Di Giuseppe[1], Chiara Cagnazzo[2], Chris Barnard[1]

[1]European Centre for Medium-Range Weather Forecasts, Reading, RG29AX, UK
[2]European Centre for Medium-Range Weather Forecasts, Robert-Schuman-Platz 3, 53175 Bonn, Germany

Correspondence to: Joe McNorton (joe.mcnorton@ecmwf.int)

Abstract. Fire is a key component of the Earth system, influencing ecosystems, atmospheric composition, and carbon–climate feedbacks. Although observations, process-based models, and data-driven approaches have advanced understanding of historical global fire activity, projecting fire regimes under concurrent changes in climate, fuels, land cover, and socioeconomic conditions remains challenging. Here, we present Sparky-Climate, a data-driven framework providing a global reconstruction and scenario-based projections of burned area and eight fuel characteristics from 1950 to 2100 at monthly approximately 25 km resolution. The framework emulates fuel load, vegetation state, and fuel moisture before predicting burned area fraction from meteorological, land-cover, fuel, and socioeconomic predictors. Historical reconstructions are driven by reanalysis and historical socioeconomic data, whereas future projections use CMIP6 climate simulations with Shared Socioeconomic Pathway-consistent land-use and socioeconomic inputs.

Comparison with the FireCCILT11 satellite-based burned area product shows agreement in spatial patterns, temporal variability, and multi-decadal trends (r = 0.87). By the late 21st century, global burned area is projected to decline by 6.7–21.9% across the scenario ensemble, masking substantial regional divergence. Savanna burned area is projected to decline by 15.2–31.3%, whereas temperate and boreal forests are projected to increase by 6.3–18.2%, particularly under high-emission pathways. Tropical moist forests are projected to show weak declines under low-emission pathways (7.6–8.1%) but increases under high-emission pathways (7.6–24.4%). Extreme fire activity is projected to decline in tropical regions, but to increase in temperate and boreal biomes, with the strongest amplification generally occurring for the most extreme events and under higher-emission scenarios.

Sparky-Climate provides a consistent framework for analysing long-term changes in fuel conditions and fire regimes under alternative climate and socioeconomic pathways.

1 Introduction

Fire is a fundamental ecological process that influences ecosystem dynamics, society, atmospheric composition, and carbon–climate feedbacks across the globe (Andela et al., 2017; Bistinas et al., 2014). Climatic conditions such as temperature,

https://doi.org/10.5194/egusphere-2026-5374
Preprint. Discussion started: 16 September 2026

precipitation, humidity, and wind govern fire weather by affecting fuel dryness and potential fire spread, as represented by indices such as the Canadian Fire Weather Index (Van Wagner, 1974). Climate also regulates fuel dynamics through its effects on vegetation growth, biomass accumulation, and phenology, thereby influencing the amount and condition of biomass available for combustion. Fire regimes additionally respond to human drivers, including ignition sources, land-use change, landscape fragmentation, suppression, and socioeconomic development, which can amplify or dampen fire activity independently of climatic change (Andela et al., 2017; Kelley et al., 2019).

Observed and reconstructed burned area records have documented substantial changes in global fire activity in recent decades, including an overall decline in global burned area (Andela et al., 2017; Zheng et al., 2021). However, this global mean trend masks substantial regional heterogeneity, with contrasting trends and increasing fire activity, fire-weather favourability, or fire risk reported in parts of the boreal, temperate, and tropical forest zones (Jolly et al., 2015; Jones et al., 2022). Understanding these divergent responses requires consideration of interactions among climate, fuel availability and moisture, land-use change, human ignitions, accessibility, and fire-management capacity.

At a global scale a range of approaches has been developed to investigate historical and future changes in fire activity. Dynamic global vegetation models (DGVMs) and Earth system models (ESMs) represent interactions among vegetation, climate, and fire and, in some cases, include land-use change and human influences (Li et al., 2019; Perkins et al., 2024). Fire-weather indices and climate-driven projections provide complementary assessments of changing conditions conducive to fire (El Garroussi et al., 2024; Gallo et al., 2025; Quilcaille et al., 2023). These approaches have provided important insight into fire-climate interactions, but their treatment of fuel dynamics, land use, and human activity varies substantially among models and applications.

Recent statistical and machine-learning studies have also reconstructed historical global burned area using climatic, vegetation, and socioeconomic predictors (Guo et al., 2025; Lampe et al., 2026). These studies demonstrate the potential of data-driven methods to reproduce observed spatial patterns, seasonality, and interannual variability, and to extend burned area estimates beyond the satellite era. However, their primary focus is historical reconstruction. Extending such approaches to the future requires scenario-consistent representations of climate, land cover, socioeconomic change, and evolving fuel conditions, while accounting for uncertainty associated with climate-model forcing. A framework that represents fuel state explicitly is particularly relevant because changes in fuel amount and moisture can mediate, offset, or amplify the effects of changing fire weather.

Here, we develop Sparky-Climate, a data-driven framework that produces monthly global estimates of eight fuel characteristics and burned area at approximately 25 km resolution for 1950–2100. Previous components of the Sparky framework were developed for fuel estimation, fire forecasting, and early-warning applications (Di Giuseppe et al., 2025; McNorton & Di

https://doi.org/10.5194/egusphere-2026-5374
Preprint. Discussion started: 16 September 2026

Giuseppe, 2024; McNorton et al., 2024). Sparky-Climate extends this work by coupling emulated fuel states with burned area prediction. It uses separate backward and forward fuel models to reconstruct historical conditions and generate scenario-based projections using harmonised reanalysis, CMIP6 climate simulations, land-use projections, and socioeconomic pathways. The framework uses climate, vegetation, land-cover, and socioeconomic variables jointly to represent predictive relationships with fuel characteristics and burned area.

This study has three objectives: (1) to develop and evaluate a globally consistent framework for reconstructing and projecting fuel characteristics and burned area; (2) to assess its ability to reproduce observed spatial patterns, temporal variability, and multi-decadal burned area trends using an observationally independent product and a temporally out-of-sample period; and (3) to characterise projected changes in burned area, fuel conditions, and extreme fire activity across major biomes and climate–socioeconomic scenarios. Sparky-Climate provides a consistent basis for fire-regime analysis, carbon-emissions modelling, climate-impact assessment, and investigations of long-term wildfire hazard and exposure. Its projections are scenario-based estimates conditional on the assumed climate, land-use, and socioeconomic pathways, rather than causal attribution of individual drivers.

2 Methods

2.1 Overview and Modelling Framework

Sparky-Climate provides monthly global estimates of eight fuel characteristics and burned area at approximately 25 km resolution. The dataset comprises a historical reconstruction for 1950–2022 and scenario-based projections for 2015–2100. The overlap period allows comparison between simulations driven by reanalysis and climate-model forcing. The workflow consists of three stages. First, the preparation and harmonisation of target and predictor data. Second, training of fuel and burned area models and finally, evaluation against an observationally independent burned area product (Fig. 1).

Sparky-Climate uses eXtreme Gradient Boosting (XGBoost) regression models (Chen and Guestrin, 2016) to emulate monthly fuel characteristics and predict burned area. The framework first estimates fuel state, including fuel load and moisture, from meteorological and land-cover inputs. These estimates are then combined with meteorological, land-cover, and socioeconomic predictors to estimate burned area. Socioeconomic variables are included as proxies for human presence, development, accessibility, and land-management conditions. They are used to capture predictive associations with ignition pressure, landscape fragmentation, and suppression capacity, but are not interpreted as direct or independently causal controls on burned area.

The fuel characteristics are modelled using a squared-error objective. High (forests) and low (grasses) vegetation classes are treated as categorical predictors using the XGBoost categorical-feature option, with classes defined following Boussetta et al.

https://doi.org/10.5194/egusphere-2026-5374
Preprint. Discussion started: 16 September 2026

(2021). Separate fuel-model configurations are used for historical reconstruction and future projection because they use different temporal information pathways. The forward model uses meteorological and land-cover predictors for the current month together with modelled fuel states from the previous month to estimate current-month fuel characteristics. This configuration generates projections for 2015–2100. The backward model uses current-month predictors together with modelled fuel states from the subsequent month to reconstruct prior fuel characteristics, allowing reconstruction to proceed backwards from the observation-constrained period to 1950. The models are trained separately because their predictor structures are not temporally reversible.

Fuel models are trained using 2015–2022 target data, as described in Section 2.2.1. Hyperparameters were selected to balance model flexibility, generalisation, and computational cost at global scale with 800 estimators, a learning rate of 0.05, and a maximum tree depth of 8.

A multiplicative mean-state adjustment is applied to each fuel variable after prediction. Scaling factors are calculated as the ratio of observed to modelled mean values over the 2015-2022 period that observation data are available and applied across the full 1950–2100 simulation period. This adjustment corrects first-order mean bias while retaining simulated temporal variability and trends. The mean grid cell specific scaling factor is 0.93 ± 0.11, indicating a low overall model bias.

Burned area fraction is predicted using an XGBoost model with a Tweedie objective at the Poisson boundary. This objective was selected because it produced non-negative predictions and performed well for the highly right-skewed and zero-dominated distribution of monthly burned area fraction. The burned area model is trained using 2015–2024 data, as described in Section 2.2.1. Hyperparameters differ from those used for the fuel models to account for the greater intermittency and stochasticity of burned area dynamics. A learning rate of 0.005 is used to stabilise optimisation and reduce sensitivity to sparse, high-magnitude fire events. The number of boosting rounds is increased to 1,000 to compensate for the smaller incremental contribution of individual trees and allow the model to learn non-linear interactions among fuel availability, meteorological conditions, vegetation structure, and socioeconomic predictors. Maximum tree depth is retained at 8 to represent regionally distinct fire regimes and interactions while constraining model complexity.

For future simulations, separate fuel and burned area models are fitted using SSP2-4.5 forcing from the corresponding ESM. Fuel models are fitted over 2015–2022 and burned area models over 2015–2024 before application to the model-specific future scenario. SSP2-4.5 was selected as an intermediate pathway judged most suitable for approximating observed forcing over the respective training periods. This approach allows the machine-learning framework to accommodate systematic differences between individual ESM forcings and reanalysis before application to their corresponding future scenarios.

https://doi.org/10.5194/egusphere-2026-5374
Preprint. Discussion started: 16 September 2026

2.2 Training and predictor data

2.2.1 Fuel and burned area targets

The eight fuel targets comprise leaf area index (LAI), live leaf mass, live wood mass, dead foliage mass, dead wood mass, live fuel moisture content, dead foliage moisture content, and dead wood moisture content. LAI is obtained from the Copernicus Land Monitoring Service (CLMS-LAI, 2025). Annual ESA-CCI above-ground biomass estimates are used to derive live and dead fuel-load targets, which are temporally disaggregated and assigned to fuel classes using Sparky-Fuel (McNorton and Di Giuseppe, 2024; Santoro et al., 2024). Fuel-moisture targets are derived using Sparky-Fuel, ERA5-Land meteorological forcing, and time-varying land cover (McNorton and Di Giuseppe, 2024; Muñoz-Sabater et al., 2021; Tourigny et al., 2025). All fuel targets are regridded or generated at the monthly 25 km target resolution. Further details of the derivation of non-LAI fuel targets are provided by McNorton and Di Giuseppe (2024). Fuel models are trained over 2015–2022, the period during which ESA-CCI biomass, LAI observations, and the datasets required to construct the fuel targets overlap.

Burned area fraction is derived from the MODIS Collection 6.1 burned area product (MCD64A1; Giglio et al., 2018) and aggregated to monthly values at the target resolution. MCD64A1 applies a hybrid algorithm that combines active-fire detections, surface reflectance, and vegetation-index information from the Terra and Aqua satellites to estimate burned area. The product identifies the spatial extent of fire-affected land from changes in surface reflectance but may be affected by temporal retrieval lags and omission of burned areas under cloud cover or dense vegetation canopies. The burned area model is trained over 2015–2024. This longer period, relative to the fuel, is possible because MCD64A1 extends beyond the ESA-CCI biomass record used to construct the fuel targets. Fuel characteristics used as burned area predictors during 2023–2024 are generated by the trained fuel models and are therefore not directly constrained by ESA-CCI biomass observations. Thus, 2015–2022 is the shared training period for the fuel and burned area components, whereas 2023–2024 extends only burned area-model training.

Table 1 lists all model predictors, grouped into meteorological, land-cover, and ancillary variables. Appendix A1 summarises the target variables, sources, temporal coverage, and processing steps.

2.2.2 Historical predictor data

Historical fuel reconstructions for 1950–2022 are driven by monthly ERA5 meteorological fields. Predictor variables include 2 m air temperature, 2 m relative humidity, precipitation, wind speed, incoming shortwave radiation, soil moisture and surface pressure. These variables represent climatic controls on photosynthesis, vegetation growth, phenology, and fuel moisture.

Land cover is represented using ECLand high- and low-vegetation fractions and vegetation classes (Boussetta et al., 2021). Time-varying land-cover data are obtained through the CERISE project and regridded to the target grid at annual resolution

https://doi.org/10.5194/egusphere-2026-5374
Preprint. Discussion started: 16 September 2026

(Tourigny et al., 2025). Static predictors comprise latitude, longitude, and orography from the ECMWF operational forecasting system (Boussetta et al., 2021). Calendar month is included to represent seasonal phenology. Grid-cell-specific 5th and 95th percentiles of 2 m temperature and precipitation, calculated from ERA5 over 2003–2024, are included to represent local climatic context.

Historical burned area reconstructions use the corresponding meteorological, land-cover, and static predictors, together with target-month modelled fuel characteristics and socioeconomic variables. Population density, gross domestic product (GDP) per capita, Human Development Index (HDI), and road length are used as proxies for human presence, development, accessibility, and potential land-management conditions. These variables may be associated with multiple and potentially opposing fire-related processes, including ignition opportunity, landscape fragmentation, and fire-management capacity.

Population density is obtained from the gridded reconstruction of Zhuang et al. (2024), which provides approximately 1 km estimates at 10-year intervals from 1950 to 2100. Values are linearly interpolated to annual resolution, area-weighted, and bilinearly interpolated to the target grid.

GDP per capita for 1990–2022 is obtained from the 5 arc-minute gridded dataset of Kummu et al. (2025) and interpolated to the target grid. Values before 1990 are reconstructed using national PPP-adjusted GDP time series from the Penn World Table (Feenstra et al., 2015). For each country, annual GDP is expressed relative to its 1990 value, and this ratio is applied to the gridded 1990 GDP field. This preserves the 1990 within-country spatial distribution while scaling values according to national historical GDP change. The method assumes temporally invariant subnational GDP distributions before 1990.

HDI is obtained from the SSP-consistent reconstruction of Liu et al. (2024), which provides national estimates at five-year intervals from 1970 to 2100. Values are linearly interpolated to annual resolution and extended to 1950 using an HDI-dependent increment function fitted to national changes during 1970–2015. National values are assigned to target-grid cells using a country mask; consequently, the dataset does not represent within-country variation in HDI.

Road length is derived from the 2018 Global Roads Inventory Project dataset (GRIP; Meijer et al., 2018), regridded from its native resolution to the target grid. As no globally consistent annual road dataset is available over the full study period, annual road length for 1950–2100 is estimated using an XGBoost model with population density, GDP, HDI, latitude, and longitude as predictors. The resulting road-length series is therefore interpreted as a modelled accessibility proxy rather than a direct observation of historical or future road networks.

https://doi.org/10.5194/egusphere-2026-5374
Preprint. Discussion started: 16 September 2026

2.2.3 Projected predictor data

Projected simulations used the same predictor structure as the historical framework but replaced historical meteorological, land-cover, and socioeconomic inputs with scenario-consistent projections. Candidate ESMs were selected from the Coupled Model Intercomparison Project Phase 6 (CMIP6) archive (Eyring et al., 2016). An ESM–scenario combination was retained only when the required variables were available for the simulation periods used for model fitting and projection. These variables comprised top-layer soil moisture, 2 m air temperature, near-surface humidity, total precipitation, wind speed, incoming shortwave radiation, and surface pressure.

Future scenarios were restricted to combinations for which climate, land use, population, gross domestic product (GDP), and Human Development Index (HDI) data could be aligned consistently (Table A2). This restriction avoided combining drivers based on incompatible scenario assumptions. Data were accessed through the Copernicus Climate Data Store and the Earth System Grid Federation via the Rook Web Processing Service. Fifteen ESMs met the variable-availability criteria (Table A3).

CMIP6 data were regridded to the target grid using bilinear or conservative interpolation, as appropriate, and processed for 2015–2100. Variables were converted to the physical quantities and units used by the corresponding ERA5 predictors (Table A4). Top-layer soil moisture, reported by CMIP6 as mass per unit area, was converted to volumetric water content using the thickness of the uppermost soil layer and a water density of 1,000 kg m^{-3}. Only ESMs with uppermost soil-layer thicknesses between 5 and 10 cm were retained, consistent with the approximately 7 cm ERA5 upper soil layer. CMIP6 shortwave-radiation fluxes were converted to provide daily accumulated energy, consistent with ERA5. Precipitation fluxes were multiplied by 86,400 s d^{-1} and divided by 1,000 kg m^{-3} to obtain precipitation depth in m d^{-1}. Near-surface specific humidity was converted to relative humidity where required. Fields reported at 1.5 m were treated as equivalent to 2 m fields.

Projected land cover and vegetation type were derived from harmonised land-use projections (Hurtt et al., 2020). Annual land-use states were mapped to ECLand vegetation classes based on vegetation characteristics. Population and HDI followed the SSP-consistent datasets described above. SSP-specific gridded GDP was obtained from Wang and Sun (2022) and interpolated to annual resolution. These socioeconomic variables were used to generate scenario-specific road-length estimates using the road model described above.

CMIP6 simulations have been evaluated against reanalysis datasets, including ERA5, and generally reproduce the large-scale spatiotemporal variability of near-surface meteorological variables relevant to vegetation growth and fire activity (IPCC, 2021; Kim et al., 2020; Li et al., 2021; Thorarinsdottir et al., 2020). Nevertheless, systematic biases remain, particularly at regional scales. CMIP6 forcing was therefore used as a scenario extension of the historical reanalysis-driven framework rather than as

https://doi.org/10.5194/egusphere-2026-5374
Preprint. Discussion started: 16 September 2026

a bias-free representation of observed meteorological conditions. Projections should be interpreted as scenario-based estimates conditional on the selected ESMs and assumed land-use and socioeconomic pathways.

2.3 Evaluation data

Model performance was evaluated using the FireCCILT11 global burned-area product (Otón et al., 2021). FireCCILT11 provides monthly burned-area estimates from 1982–2018, excluding 1994, derived from the Advanced Very High Resolution Radiometer Long-Term Data Record (AVHRR-LTDR). Burned area is retrieved at 0.05° resolution and provided at 0.25° resolution, allowing comparison with Sparky-Climate after regridding to a common grid.

FireCCILT11 is observationally independent of the MODIS Collection 6.1 burned-area product (MCD64A1) used to train the model because it is derived from a different satellite record, overpass configuration, and retrieval methodology. This reduces the likelihood of artificial agreement arising from shared observations or retrieval algorithms. Its multi-decadal record also extends into the pre-MODIS period, enabling assessment of long-term spatial patterns, temporal variability, and trends.

The 2003–2014 period provides a temporally out-of-sample evaluation because it precedes both the fuel-model training period (2015–2022) and burned-area-model training period (2015–2024). The 2015–2018 overlap provides an additional comparison with an observationally independent product but is not treated as an independent temporal validation.

FireCCILT11 is subject to uncertainties associated with cloud contamination, spatial-resolution limitations, omission of small fires, and potential temporal inconsistencies linked to satellite orbit drift (Chen and Giglio, 2025; Giglio and Roy, 2022). Nevertheless, it provides one of the few globally consistent multi-decadal burned-area records available for evaluating historical fire variability and is therefore used as the primary benchmarking dataset.

2.4 Analysis of burned area and extremes

Long-term changes in reconstructed annual global burned area were characterised using a piecewise changepoint analysis. The analysis identified periods with distinct mean burned area, linear trends, and interannual variability. Changepoints were applied to the annual reconstructed global burned-area time series for 1950–2020. Biome-level time series were subsequently examined using the resulting global periods and their biome-specific temporal behaviour.

Extreme burned area was evaluated using biome-specific thresholds derived from the distribution of gridded monthly burned area during the 2015–2024 reference period. Thresholds corresponding to the 90th, 95th, 99th, and 99.9th percentiles were calculated separately for each biome using all valid grid-cell monthly values. Fractional burned area was converted to physical burned area using grid-cell area weighting before calculation of percentile exceedances.

https://doi.org/10.5194/egusphere-2026-5374
Preprint. Discussion started: 16 September 2026

Changes in extreme burned area were quantified as the probability of exceeding each reference threshold during a target period divided by the corresponding probability during the reference period. A probability ratio greater than one indicates more frequent exceedances than in the reference period, whereas a ratio below one indicates less frequent exceedances.

Historical changes were assessed by comparing 1950–1959 with the ERA5-driven 2015–2024 reference distribution. Future changes were assessed separately for each SSP by comparing late-century exceedance probabilities during 2090–2099 with the corresponding SSP-specific 2015–2024 baseline. This within-SSP comparison avoids directly comparing the distributions of ERA5-driven reconstructions and CMIP6-driven projections.

3 Results

3.1 Reconstructed and projected fuel characteristics

Reconstructed and projected fuel characteristics showed substantial spatial and biome-level variation over 1950–2100 (Fig. 2). Fuel-load totals were summarised using the spatial extent of contemporary biomes defined by Dinerstein et al. (2017). Consequently, these summaries describe changes within fixed contemporary biome boundaries and do not account for shifts in biome extent through time.

Across the historical reconstruction, global modelled fuel load declined by 198 Pg (26.8%) between 1950 and 2020. The largest absolute reduction occurred in Tropical and Subtropical Moist Broadleaf Forests (TMBF), where fuel load declined by 114 Pg (28%), with the strongest decreases located in the Amazon basin and additional reductions across Central Africa and Southeast Asia (Fig. 2). Net declines were also simulated for major northern forest biomes with decreases of 17 Pg (20%) from Temperate Broadleaf and Mixed Forests (TBF), 4 Pg (14%) from Temperate Conifer Forests (TCF) and 8 Pg (10%) from Boreal Forests (BF). These biome-level declines mask some heterogeneous spatial patterns, including localised increases in fuel load in temperate and boreal regions.

Future simulations showed increased global fuel load relative to 1950 under all assessed scenarios, reversing the historical decline simulated to 2020. By 2100, global fuel load increased by 190 ± 63 Pg (26%) under SSP1-2.6 and by 139 ± 42 Pg (19%) under SSP5-8.5. The magnitude and direction of projected changes varied substantially among biomes.

The largest absolute projected increases occurred in high-latitude forest systems. In BF, fuel load increased by 32 ± 38 Pg (41%) under SSP1-2.6 and by 51 ± 31 Pg (65%) under SSP5-8.5 relative to 1950. In TBF, corresponding increases were 29 ± 13 Pg (35%) and 24 ± 6 Pg (29%), respectively. In contrast, TMBF fuel load remained below its 1950 value under both scenarios, declining by 115 ± 32 Pg (29%) under SSP1-2.6 and by 154 ± 25 Pg (38%) under SSP5-8.5. Tropical Dry Broadleaf

https://doi.org/10.5194/egusphere-2026-5374
Preprint. Discussion started: 16 September 2026

Forests (TDBF) showed a more variable response, with a change of +1 ± 5 Pg (5%) under SSP1-2.6 and −3 ± 1 Pg (17%) under SSP5-8.5.

Large relative increases were also projected in non-forest biomes. Temperate Grasslands (TG) increased by 40 ± 10 Pg (373%) under SSP1-2.6 and by 44 ± 6 Pg (409%) under SSP5-8.5. Fuel load also increased in Tropical and Subtropical Grasslands and Savannas (TGS), with changes ranging from 18% to 101% across the assessed scenarios. Because biome totals were calculated using fixed contemporary biome boundaries, these increases include changes associated with projected transitions in underlying land-cover classes within grid cells. For example, increases in fuel load within a contemporary savanna biome may occur where projected land cover transitions towards a more forested vegetation class.

3.2 Evaluation of reconstructed burned area

Comparison with the observationally independent FireCCILT11 burned-area product showed that Sparky-Climate reproduced the large-scale spatial and temporal characteristics of global fire activity over 1982–2018 (Fig. 3). FireCCILT11 is derived from the AVHRR record, whereas Sparky-Climate was trained using MODIS MCD64A1 burned area for 2015–2024. The 1982–2014 period therefore provides a temporally out-of-sample evaluation, while the 2015–2018 overlap provides an additional comparison with an observationally independent product.

At the global scale, predicted mean annual burned area showed strong spatial agreement with FireCCILT11 ($r = 0.86$). Monthly global burned area also reproduced the broad temporal evolution of the FireCCILT11 record, including an increase from 1982 to approximately 2000, followed by stabilisation and a gradual decline to 2018 ($r = 0.85$). Sparky-Climate showed a systematic negative bias relative to FireCCILT11, underestimating total burned area by 22.4% across 1982–2018. The absolute bias was larger during 1982–2003 (-9.3 Mha yr^{-1}) than during 2003–2018 (-7.7 Mha yr^{-1}). Normalised variability was lower in Sparky-Climate than in FireCCILT11 ($\sigma_{\mathrm{model}}/\mathrm{mean} = 0.36$; $\sigma_{\mathrm{obs}}/\mathrm{mean} = 0.43$), and the centred root-mean-square error was 22.6%.

The two products showed comparable changes in global burned area across the main periods of the FireCCILT11 record. During 1982–2003, annual burned area increased by 2.42 Mha decade^{-1} in FireCCILT11 and by 2.50 Mha decade^{-1} in Sparky-Climate. During 2003–2018, both products showed declining trends, of -2.89 and -3.11 Mha decade^{-1}, respectively. Correlations between the products were $r = 0.75$ for 1982–2003 and $r = 0.73$ for 2003–2018. Comparable changes in long-term trends were also evident across several biomes (Fig. 3).

At the biome scale, agreement was strongest in the dominant fire-prone ecosystems. Tropical and Subtropical Grasslands and Savannas (TGS) and Flooded Grasslands and Savannas (FGS) showed spatiotemporal correlations of $r = 0.70$ and $r = 0.73$, respectively. Correlations for biome-total monthly and interannual variability were $r = 0.86$ in TGS and $r = 0.82$ in FGS.

https://doi.org/10.5194/egusphere-2026-5374
Preprint. Discussion started: 16 September 2026

Tropical and Subtropical Moist Broadleaf Forests (TMBF), the forested biome with the largest annual burned area, showed a spatiotemporal correlation of $r = 0.49$. Biome-total monthly and interannual variability was correlated at $r = 0.54$ in TMBF and $r = 0.52$ in Tropical and Subtropical Dry Broadleaf Forests (TDBF).

Performance was weakest in Deserts and Xeric Shrublands (DXS), where the spatiotemporal correlation was $r = 0.16$. In this biome, the correlation for biome-total seasonality was $r = 0.51$, whereas the correlation for interannual variability was $r = 0.20$. Variability was lower in Sparky-Climate than in FireCCILT11 ($\sigma_{\text{model}}/\text{mean} = 0.10$; $\sigma_{\text{obs}}/\text{mean} = 0.47$).
Overall, Sparky-Climate reproduced the dominant global spatial distribution of burned area, including major fire regions in Africa, northern Australia, and South America (Fig. 3a), as well as the principal global and biome-level seasonal, interannual, and multi-decadal patterns represented in FireCCILT11.

3.3 Reconstructed burned area

Global reconstructed burned area showed distinct periods of differing mean conditions, trends, and interannual variability between 1950 and 2020 (Fig. 4; A1-2). A piecewise changepoint analysis of annual burned area identified four periods. During 1950–1971, annual burned area was relatively variable (mean = 369 Mha yr^{-1}; σ = 32 Mha) and declined at −2.9 Mha yr^{-1} per year. This was followed by a period of comparatively low and stable annual burned area during 1972–1989 (mean = 323 Mha yr^{-1}; σ = 8.8 Mha; trend = +0.03 Mha yr^{-1} per year). Burned area increased during 1990–1999 (mean = 338 Mha yr^{-1}; σ = 20 Mha; trend = +5.00 Mha yr^{-1} per year), before entering a period of elevated but declining burned area between 2000 and 2020 (mean = 378 Mha yr^{-1}; trend = −1.39 Mha yr^{-1} per year).

The reconstructed global trajectory was reflected most clearly in Tropical and Subtropical Grasslands and Savannas (TGS), which accounted for approximately 70% of global burned area (Figs. 5 and 6). TGS showed high interannual variability during 1950–1967, followed by a lower-burning period from 1967 to 1990. Burned area subsequently increased until approximately 2000 and declined thereafter. The contribution of TGS to global burned area decreased from 74% during 1950–1971 to 68% during 2000–2020.

Tropical and Subtropical Moist Broadleaf Forests (TMBF), which represented the largest contribution to forested burned area, showed some divergence from the global pattern. Although the early high-burning period (1950–1967) was evident, the subsequent low-burning phase (1967–1999) was more prolonged than in the global and savanna time series. Burned area increased around the turn of the 21st century by +1.9 Mha yr^{-1} (+8%) in TMBF, compared with +3.9 Mha yr^{-1} (+1.5%) in TGS. Subsequent declines were −3% yr^{-1} in TMBF and −2% yr^{-1} in TGS.

Other biomes showed weaker correspondence with the global trajectory. In Deserts and Xeric Shrublands (DXS), reconstructed burned area shifted from relatively high to lower values around 1970, followed by a long period of comparatively stable but

https://doi.org/10.5194/egusphere-2026-5374
Preprint. Discussion started: 16 September 2026

variable conditions. Temperate Grasslands (TG), Tropical and Subtropical Dry Broadleaf Forests (TDBF), and Boreal Forests (BF) showed weaker alignment with the global pattern and no consistent decline after 2000.

3.4 Projected burned area

Projected global burned area diverged among SSP scenarios from 2015 to 2099, although all scenarios showed a long-term decline relative to the 2020s baseline (Fig. 4; Table 2). By 2090–2099, ensemble-mean burned area declined by 21.9% under SSP1-1.9, 21.5% under SSP1-2.6, and 20.2% under SSP2-4.5. Smaller late-century reductions were simulated under SSP4-3.4 (13.0%), SSP3-7.0 (6.8%), and SSP5-8.5 (13.5%).

The largest reductions occurred during 2025–2049, when ensemble-mean trends ranged from −2.5 Mha yr^{-1} per year under SSP1-1.9 to −0.9 Mha yr^{-1} per year under SSP3-7.0. By 2045–2054, this corresponded to reductions of approximately 17.5% to 6.7% relative to the 2020s baseline. Under SSP1-1.9, SSP1-2.6, and SSP2-4.5, declining trends persisted after 2050 before tending towards stabilisation. Under SSP4-3.4, burned area stabilised after 2050 with no clear trend. Under SSP3-7.0 and SSP5-8.5, burned area stabilised during the mid-century period before weak positive trends emerged after 2072 and 2062, respectively. Late-century trends were +0.4 Mha yr^{-1} per year under both SSP3-7.0 and SSP5-8.5, corresponding to increases of approximately 3–5% relative to the mid-century minimum.

The CMIP6 ensemble showed broad agreement on the direction of long-term global change within each scenario. Inter-model standard deviations in long-term trend magnitude were approximately 0.17–0.25 Mha yr^{-1} per year under low- and intermediate-emission pathways. Spread was larger under SSP3-7.0 and SSP5-8.5, where ensemble-mean trends were -0.39 ± 0.30 and -0.65 ± 0.39 Mha yr^{-1} per year, respectively. One model simulated a weakly positive overall trend under SSP3-7.0.

Inter-model spread in absolute annual burned area remained broadly stable through time. During the 2020s, ensemble-mean annual burned area ranged from 307 to 345 Mha yr^{-1} across SSPs, with relative standard deviations of 8.9–13.7% among ensemble members within each scenario. By the 2090s, ensemble means ranged from 284 to 325 Mha yr^{-1} and relative standard deviations ranged from 8.6% to 14.6%.

Biome-level projections differed substantially from the global mean response (Fig. 6). Tropical and Subtropical Grasslands and Savannas (TGS), which accounted for approximately 70% of global burned area, showed declining burned area in all CMIP6 models and SSP scenarios. Ensemble-mean long-term trends ranged from -1.01 ± 0.17 Mha yr^{-1} per year under SSP2-4.5 to -0.53 ± 0.18 Mha yr^{-1} per year under SSP3-7.0. Relative inter-model spread was approximately 14–28% in most scenarios and was largest under SSP3-7.0 (34%).

https://doi.org/10.5194/egusphere-2026-5374
Preprint. Discussion started: 16 September 2026

TGS declines were strongest during 2025–2049, with trends of −2.31 Mha yr^{-1} per year under SSP1-1.9 and −2.08 Mha yr^{-1} per year under SSP1-2.6. During 2075–2099, negative trends persisted in all scenarios except SSP3-7.0, ranging from −0.14 Mha yr^{-1} per year under SSP4-3.4 to −0.31 Mha yr^{-1} per year under SSP1-2.6; the SSP3-7.0 trend was +0.01 Mha yr^{-1} per year. By 2090–2099, TGS burned area declined by 31% under SSP1-1.9 and SSP1-2.6, 30% under SSP2-4.5, and 27% under SSP5-8.5, relative to the 2020s. Smaller reductions were simulated under SSP4-3.4 (21%) and SSP3-7.0 (15%). Ensemble-mean annual burned area declined from approximately 184–227 Mha yr^{-1} during the 2020s to 149–189 Mha yr^{-1} by late century.

Tropical and Subtropical Moist Broadleaf Forests (TMBF), which accounted for approximately 10% of total burned area and had the largest burned area of any forest biome, showed greater inter-model and scenario-dependent variation. Ensemble-mean trends during 2020–2099 were weakly negative under SSP1-1.9 and SSP1-2.6 (−0.035 to −0.030 Mha yr^{-1}). Under SSP2-4.5, the trend was −0.016 ± 0.038 Mha yr^{-1}. Positive ensemble-mean trends occurred under SSP3-7.0 (+0.10 ± 0.09 Mha yr^{-1}) and SSP5-8.5 (+0.08 ± 0.09 Mha yr^{-1}).

During 2025–2049, TMBF burned area declined by −0.06 Mha yr^{-1} per year under SSP1-1.9 and by −0.07 Mha yr^{-1} per year under SSP1-2.6. In contrast, trends were +0.00 Mha yr^{-1} per year under SSP5-8.5 and +0.05 Mha yr^{-1} per year under SSP3-7.0. By the 2090s, TMBF burned area was 8% lower than the 2020s baseline under SSP1-1.9 and SSP1-2.6 and 4% lower under SSP2-4.5. It was higher than the 2020s baseline by 24% under SSP3-7.0, 8% under SSP4-3.4, and 21% under SSP5-8.5. Tropical and Subtropical Dry Broadleaf Forests (TDBF) showed small-magnitude ensemble-mean trends across scenarios, ranging from −0.01 to +0.03 Mha yr^{-1}. Changes by the 2090s were typically between −5% and +5% relative to the 2020s baseline. SSP5-8.5 showed a larger late-century increase of 18%.

Temperate Broadleaf and Mixed Forests (TBF) and Boreal Forests (BF) showed positive ensemble-mean trends across all SSPs. In TBF, late-century trends ranged from +0.003 to +0.026 Mha yr^{-1}, corresponding to end-of-century increases of 1% under SSP1-1.9 to 16% under SSP5-8.5 relative to the 2020s baseline. BF trends ranged from +0.006 to +0.020 Mha yr^{-1}, corresponding to increases of 4% under SSP1-1.9 to 18% under SSP5-8.5. All BF ensemble members showed positive trends except for one SSP2-4.5 simulation. Under higher-emission pathways, much of the projected increase in TBF and BF occurred after 2050.

Overall, projected burned-area trajectories differed markedly between forested and non-forested biomes. TGS showed consistent declines under all scenarios, whereas TMBF responses varied among scenarios and models, and TBF and BF showed consistent increases.

https://doi.org/10.5194/egusphere-2026-5374
Preprint. Discussion started: 16 September 2026

3.5 Changes in extreme wildfires

Historical and projected changes in extreme burned area were strongly biome dependent (Fig. 7). Historical probability ratios compare exceedance frequencies during 1950–1959 with the ERA5-driven 2015–2024 reference period. In Tropical and Subtropical Grasslands and Savannas (TGS), the probability of exceeding the 99.9th-percentile burned-area threshold was approximately 1.05 times higher during the 1950s than during the reference period. This increase was smaller than the corresponding increases at lower percentile thresholds. In Deserts and Xeric Shrublands (DXS) and Flooded Grasslands and Savannas (FGS), 99.9th-percentile exceedances were approximately 1.53 and 2.42 times more frequent, respectively, during 1950–1959.

Historical patterns differed among forest biomes. The probability of exceeding the 99.9th-percentile threshold during the 1950s was lower in Tropical and Subtropical Moist Broadleaf Forests (TMBF; probability ratio = 0.70) and Boreal Forests (BF; 0.45), but higher in Tropical and Subtropical Dry Broadleaf Forests (TDBF; 1.14) and Temperate Broadleaf and Mixed Forests (TBF; 2.11).

Projected late-century changes in extreme burned area were also strongly biome and scenario dependent. In TGS, TMBF, DXS, and TDBF, 99th- and 99.9th-percentile exceedances declined across all scenarios. In TGS, the probability of exceeding the 99.9th-percentile threshold declined to 0.08, 0.10, and 0.03 times the corresponding SSP-specific 2015–2024 baseline under SSP3-7.0, SSP4-3.4, and SSP5-8.5, respectively. Under lower-emission pathways, the frequency of 99.9th-percentile exceedances also declined by at least 80% relative to the SSP-specific baseline. Reductions were smaller at lower percentile thresholds.

In TMBF, probabilities of exceeding the 99th- and 99.9th-percentile thresholds declined to between 0.16 and 0.47 times the SSP-specific contemporary baseline across scenarios. In contrast, exceedance probabilities at the 90th and 95th percentiles increased under higher-emission pathways, reaching 1.15–1.56 times the baseline frequency.

Temperate and boreal biomes generally showed increased probabilities of extreme burned-area exceedance across percentile thresholds and scenarios. Probability ratios ranged from 1.02 to 1.84 and were generally largest at higher percentiles and under SSP5-8.5. The exception was TBF under SSP1-1.9, where the probability of exceeding the 99.9th-percentile threshold was 0.91. In BF, probability ratios under SSP1-2.6 increased from 1.15 at the 90th percentile to 1.63 at the 99.9th percentile. Under SSP5-8.5, the corresponding probability ratios were 1.29 and 1.84.

https://doi.org/10.5194/egusphere-2026-5374
Preprint. Discussion started: 16 September 2026

4 Discussion

4.1 Harmonised reconstruction and projection of burned area

This study presents a scenario-consistent framework for reconstructing and projecting monthly global fuel characteristics and burned area at ~25 km resolution from 1950 to 2100. The framework combines reanalysis-driven historical reconstructions with CMIP6-driven future simulations within a common empirical modelling architecture. Its primary contribution is therefore not the introduction of a wholly new fire driver or the first global analysis of burned-area change. Rather, it provides a spatially explicit and internally harmonised dataset that links reconstructed and projected fuel conditions with burned-area simulations across historical and future periods.

Previous studies have documented long-term changes in global burned area and their substantial regional variation using satellite observations, reconstructions, dynamic global vegetation models, and Earth system models (e.g. Andela et al., 2017; Guo et al., 2025; Lampe et al., 2026). Other work has demonstrated the importance of climate, fire weather, vegetation, land use, and human activity in shaping fire regimes (Bowman et al., 2011; Jolly et al., 2015; Jones et al., 2022). Sparky-Climate builds on this evidence by combining a broad set of time-varying predictors within a single framework. In particular, the framework first reconstructs and projects eight fuel characteristics representing fuel load, vegetation structure, and live and dead fuel moisture, and then uses the resulting contemporaneous fuel states alongside meteorological, land-cover, and socioeconomic predictors to simulate burned area.

The socioeconomic representation includes population density, gridded GDP, HDI, and modelled road length. Together, these variables provide complementary proxies for human presence, development, access, land management, ignition opportunity, and potential suppression capacity. They should not, however, be interpreted as direct measures of individual fire-management processes or as enabling causal attribution of their separate effects. Although previous global studies have incorporated one or more human or land-use variables, the combined representation of multiple socioeconomic predictors with explicitly modelled, time-varying fuel states is a central feature of Sparky-Climate. The use of harmonised historical trajectories and SSP-consistent future pathways for these variables, together with land cover and meteorological forcing, allows their co-evolution to be represented from 1950 to 2100.

A further contribution is the harmonisation of historical reconstruction and future projection within a common modelling architecture. Fuel and burned-area simulations use consistent predictor definitions, spatial resolution, output variables, and sequential fuel-to-burned-area structure across the ERA5-driven historical and SSP-driven future periods. This reduces discontinuities that can arise when historical and future fire estimates are generated using separate datasets, models, or variable definitions, and allows changes across the full 1950–2100 period to be examined within a consistent framework.

https://doi.org/10.5194/egusphere-2026-5374
Preprint. Discussion started: 16 September 2026

A further feature of the projection framework is the use of ESM-specific fuel and burned-area models. These models are fitted using forcing from the corresponding ESM before application to its future simulations, allowing statistical relationships to be learned within the meteorological forcing space of each climate model. This approach is intended to accommodate systematic differences between ERA5 and individual ESM simulations, rather than assuming that CMIP6 fields provide bias-free representations of observed meteorological conditions. It does not, however, remove uncertainty associated with climate-model structure, scenario assumptions, or extrapolation beyond the model-fitting period.

Comparison with the observationally independent FireCCILT11 burned-area product indicates that the framework reproduces major global spatial patterns, seasonal and interannual variability, and the broad multi-decadal evolution of burned area. The 1982–2014 comparison provides temporally out-of-sample evidence of model performance, while the 2015–2018 comparison remains independent in terms of the satellite product but overlaps the MODIS training period. The systematic negative bias relative to FireCCILT11 and weaker performance in Deserts and Xeric Shrublands show that model skill is not uniform among fire regimes. Accordingly, the dataset is best interpreted as a scenario-based reconstruction and projection tool for examining large-scale patterns and associations among changing fuel conditions, climate, land cover, and socioeconomic proxies, rather than as a causal attribution framework or a bias-free representation of specific historical and future fire activity.

4.2 Reconstructed burned area trends

The reconstructed historical record indicates that global burned area did not follow a single monotonic trajectory between 1950 and 2020. Instead, it comprised successive periods of decline, relative stability, increase, and subsequent decline. At the global scale, reconstructed burned area declined during 1950–1971, remained comparatively low and stable from 1972–1989, increased during 1990–1999, and declined again after 2000. The most recent declining phase is supported by the observational record. Sparky-Climate reproduces the direction and approximate magnitude of the FireCCILT11 trends during both 1982–2003 and 2003–2018. More specifically, both datasets show increasing burned area before the early 2000s and declining burned area thereafter. This agreement supports the interpretation that the recent global decline is not solely an artefact of the reconstruction framework.

The reconstructed sequence of alternating global fire regimes is also broadly consistent with other long-term global burned-area reconstructions. Guo et al. (2025) reported a long-term decline during the early twentieth century, followed by increasing burned area towards the early 2000s and a subsequent decline. Lampe et al. (2026) likewise identified substantial multi-decadal variability rather than a uniform long-term global trend. The timing, magnitude, and attribution of individual phases differ among products, as expected from differences in training data, temporal coverage, predictors, spatial resolution, and model structure. Nevertheless, the agreement that global burned area exhibits substantial multi-decadal variability provides useful context for the reconstructed changes presented here.

https://doi.org/10.5194/egusphere-2026-5374
Preprint. Discussion started: 16 September 2026

The historical trajectory was most strongly expressed in Tropical and Subtropical Grasslands and Savannas (TGS), which accounted for approximately 70% of global burned area. The decline in the TGS contribution from 74% of global burned area in 1950–1971 to 68% in 2000–2020 indicates a relative redistribution of global burned area away from the principal savanna fire regimes. This pattern is consistent with evidence that recent global burned-area declines have been concentrated in African and other savanna-dominated landscapes, where changes in land use, agricultural expansion, settlement, and landscape fragmentation can alter the continuity of burnable vegetation and the opportunity for fire spread (Andela et al., 2017). These shifts, captured by Sparky-Climate, are represented through land-cover and socioeconomic proxy variables and the reconstruction does not separate their individual contributions or demonstrate causal attribution.

Tropical and Subtropical Moist Broadleaf Forests showed a partly distinct temporal evolution, including a more prolonged low-burning phase between 1967 and 1999 and a proportionally larger increase around the turn of the century than in TGS. This divergence is consistent with the contrasting environmental and human contexts of forest and savanna fire regimes. In tropical forests, burned area is commonly associated with the interaction of dry conditions, forest degradation, agricultural expansion, and ignition sources, whereas fire in savanna systems is more widespread and recurrent. The reconstructed differences should nonetheless be interpreted cautiously, because the model represents these controls statistically and does not resolve local land-management practices, deforestation pathways, or fire-use decisions explicitly.

The comparison with FireCCILT11 supports the broad spatial distribution, seasonality, and multi-decadal evolution of reconstructed burned area, while also showing systematic negative bias and reduced variability in some biomes. Agreement was strongest in Tropical and Subtropical Grasslands and Savannas and Flooded Grasslands and Savannas, which have recurrent and spatially extensive fire regimes, and weakest in Deserts and Xeric Shrublands, where the model underrepresented interannual variability. The latter result is consistent with the difficulty of representing episodic, spatially heterogeneous fires driven by intermittent fuel production and local weather at approximately 25 km monthly resolution. The limitations of the observational records, early reanalysis forcing, and temporal extrapolation are discussed in Section 4.5.

Overall, the reconstruction supports previous evidence that global fire activity has undergone substantial temporal and regional reorganisation, rather than a simple long-term increase or decrease. It also provides a coherent bridge between the pre-satellite and satellite periods. Agreement with FireCCILT11 and other long-term products supports the first-order temporal patterns and regimes identified here, but does not confirm the precise magnitude or causal drivers of historical burned-area change.

4.3 Divergent projected fire regimes across biomes

Although global burned area declined out to 2100 under all assessed SSPs, the projected response was strongly biome dependent. The global decline was driven primarily by Tropical and Subtropical Grasslands and Savannas (TGS), which account for approximately 70% of contemporary global burned area and showed declining burned area in every ESM and scenario. By late century, TGS burned area declined by 15–31% relative to the 2020s, depending on scenario. The strongest reductions occurred under SSP1-1.9 and SSP1-2.6, whereas the decline was smaller under SSP3-7.0. These results are consistent with evidence that recent global burned-area declines have been concentrated in savanna-dominated regions, particularly where agricultural expansion, settlement, and other changes in land use have altered fuel continuity and limited fire spread (Andela et al., 2017).

Within Sparky-Climate, this projected savanna decline emerges from the combined modelled relationships among meteorological conditions, land cover, fuel characteristics, and socioeconomic proxy variables. The projections are therefore consistent with an increasing influence of changing land use, landscape structure, and human activity on the extent of burned area in TGS. However, the model does not provide a formal attribution of the decline to individual predictors. In particular, population density, GDP, HDI, and road length represent correlated proxies for multiple processes, including human presence, access, land management, ignition opportunity, and suppression capacity. The declining TGS signal should consequently not be interpreted as evidence that any one of these processes is the dominant driver.

The fuel projections provide important context for this result. Fuel load increased within contemporary TGS biome boundaries under the assessed scenarios, despite the consistent decline in projected burned area. This apparent contrast reflects the fact that fuel availability alone does not determine fire extent. In addition, because biome totals were calculated within fixed contemporary biome masks, increases in fuel load within TGS may include grid cells in which the underlying projected land-cover class transitions towards more woody or forested vegetation. The combination of increasing modelled fuel load and declining burned area is thus consistent with a changing vegetation and land-use mosaic in which the spatial continuity, arrangement, and accessibility of fuels may be as important as total fuel quantity for the propagation of large fires.

Tropical and Subtropical Moist Broadleaf Forests (TMBF) showed a more uncertain response than TGS. Burned area declined slightly under low-emission pathways but increased under SSP3-7.0 and SSP5-8.5, with substantial inter-model spread in the magnitude and, in some cases, direction of change. This uncertainty occurs alongside projected declines in TMBF fuel load relative to 1950 under both SSP1-2.6 and SSP5-8.5. The combination of lower aggregate modelled fuel load and a potentially increasing burned-area response under higher-emission pathways illustrates that changes in total biomass cannot be interpreted as a direct indicator of burned-area change. Instead, the modelled relationships suggest that climate, vegetation structure, land-cover change, and socioeconomic conditions may combine differently across scenarios to produce contrasting tropical-forest fire regimes.

The projected behaviour of TMBF is broadly consistent with the sensitivity of tropical forests to interacting climatic and land-use pressures. Observational evidence has linked tropical fire occurrence to drought, forest degradation, agricultural expansion,

https://doi.org/10.5194/egusphere-2026-5374
Preprint. Discussion started: 16 September 2026

and ignition sources, while studies also indicate a weakening tropical forest carbon sink under ongoing environmental change (Hubau et al., 2020; Parry et al., 2022). Sparky-Climate does not explicitly resolve deforestation decisions, local forest-management practices, or individual ignition processes. Nevertheless, the scenario-dependent TMBF response indicates that future tropical-forest burned area may be particularly sensitive to the way these processes co-evolve with climate and vegetation conditions. Tropical and Subtropical Dry Broadleaf Forests showed comparatively small and uncertain changes in mean burned area across most scenarios, although SSP5-8.5 produced a more pronounced late-century increase. This further emphasises that tropical fire responses cannot be represented by a single regional trajectory.

In contrast, Temperate Broadleaf and Mixed Forests and Boreal Forests showed consistent increases in mean burned area across all assessed scenarios. These increases were generally modest in magnitude relative to the projected decline in savanna burning, but their direction was robust across the ESM ensemble. The largest changes occurred under SSP5-8.5, and much of the increase in temperate and boreal burned area occurred after 2050. These results are consistent with wider evidence that warming, longer fire-weather seasons, and changing vegetation conditions are increasing fire-conducive conditions across northern ecosystems (Jolly et al., 2015; Jones et al., 2022).

Projected increases in temperate and boreal burned area occurred alongside substantial increases in modelled fuel load, particularly in Boreal Forests and Temperate Broadleaf and Mixed Forests. This alignment is consistent with the possibility that changing fuel conditions and meteorological forcing jointly contribute to an increasingly fire-prone northern landscape. However, this pattern does not demonstrate a direct fuel-driven mechanism because the fuel and burned-area models are statistically linked, and the projections remain conditional on the climate, land-cover, and socioeconomic inputs. The fixed biome mask and other structural limitations of the framework are considered further in Section 4.5.

Taken together, the projections show that a declining global burned-area total can obscure a substantial redistribution of fire activity among biomes. Fire declines in savanna systems dominate the global mean because of their large present-day contribution to burned area, whereas increasing mean burned area in temperate and boreal forests becomes more evident at biome scale. This redistribution is potentially important for the carbon-cycle implications of future fire regimes because forest fires often occur in ecosystems with higher biomass stocks than the grassland and savanna systems that dominate global burned area. Quantification of resulting fire emissions, however, requires explicit evaluation of combustion completeness, fuel consumption, post-fire recovery, and associated carbon fluxes, which are outside the scope of the present burned area analysis.

Overall, Sparky-Climate projections are consistent with future fire regimes being shaped by interacting changes in climate, fuel state, land cover, and human activity rather than by a uniform global climate–fire response. The global decline in burned area should therefore not be interpreted as a uniform reduction in fire risk, particularly in temperate and boreal systems and in the upper tail of their burned-area distributions, considered next.

https://doi.org/10.5194/egusphere-2026-5374
Preprint. Discussion started: 16 September 2026

4.4 Extreme burned-area projections and high-latitude fire risk

The projected changes in extreme burned area out to 2100 reinforce the conclusion that changes in mean burned area do not fully describe future fire risk. Across tropical and savanna biomes, the upper tail of the burned area distribution generally declined, whereas Temperate Broadleaf and Mixed Forests (TBF) and Boreal Forests (BF) generally showed increasing exceedance probabilities across moderate and extreme thresholds. Across temperate and boreal biomes, probability ratios, relative to the contemporary period, ranged from 1.02 to 1.84 and were generally largest at higher percentile thresholds and under SSP5-8.5. TBF under SSP1-1.9 was the exception, with a slight reduction in the probability of exceeding the 99.9th-percentile threshold (probability ratio = 0.91).

The upper-tail increase was especially clear in BF. Under SSP1-2.6, the probability ratio increased from 1.15 at the 90th percentile to 1.63 at the 99.9th percentile; under SSP5-8.5, the corresponding values were 1.29 and 1.84. The increase in probability ratios towards the upper tail indicates that the projected change in BF is not restricted to a uniform upward shift in burned area but includes a disproportionate increase in the occurrence of the largest monthly burned area events. TBF also showed generally increasing moderate and extreme burned area exceedance probabilities across scenarios, consistent with its projected increase in mean burned area, although the response was weaker or reversed for the most extreme threshold under SSP1-1.9.

This projected high-latitude intensification is consistent with wider evidence of increasing fire-conducive conditions across northern ecosystems. Observational and modelling studies have linked recent increases in northern fire activity to warming temperatures, earlier snowmelt, longer fire seasons, more frequent or intense periods of fire weather, and changes in vegetation productivity and fuel availability (e.g. Abatzoglou and Williams, 2016; Jolly et al., 2015; Jones et al., 2022). Within Sparky-Climate, the coincident increases in projected temperate and boreal fuel loads, mean burned area, and extreme-burned-area exceedance probabilities are consistent with increasingly fire-prone northern landscapes. However, these patterns arise from the combined statistical relationships among modelled fuel states, climate forcing, land cover, and socioeconomic proxies. They do not provide a formal attribution of extreme-fire changes to individual mechanisms.

The contrast with Tropical and Subtropical Grasslands and Savannas is particularly important. Although TGS currently dominates global burned area, the probability of the most extreme monthly burned-area events declined substantially in all future scenarios. For example, 99.9th-percentile exceedance probabilities were reduced to 0.08, 0.10, and 0.03 of their SSP-specific contemporary values under SSP3-7.0, SSP4-3.4, and SSP5-8.5, respectively. This pattern suggests that declining global burned area is accompanied by a marked reduction in upper-tail activity in the biome that dominates the present-day global total. The modelled relationships are consistent with future changes in land cover, fuel configuration, and socioeconomic conditions limiting the occurrence or spatial propagation of large savanna fire events, although the present analysis does not isolate the contribution of individual predictors.

Tropical and Subtropical Moist Broadleaf Forests showed a different form of distributional change. Under higher-emission pathways, exceedances at the 90th and 95th percentiles increased, whereas 99th- and 99.9th-percentile exceedances declined across scenarios. This combination suggests that future change in this biome may not be represented adequately by mean burned area or by a single definition of extreme fire. The projected pattern is consistent with more frequent moderately large burned-area events occurring alongside a reduced frequency of the largest events. Such a response may reflect changes in the spatial arrangement of vegetation, land cover, and ignition opportunities, in combination with changing meteorological conditions, but this interpretation requires targeted attribution analysis and evaluation against independent regional observations.

The projected increases in high-latitude extreme burned area are relevant to recent severe boreal fire seasons, including those experienced in Canada during 2023 and 2024 (Jones et al., 2024a). These events illustrate the potential consequences of concurrent heat, drought, extended fire-weather seasons, and extensive available fuels in northern forest landscapes. Sparky-Climate was not evaluated specifically against these events and does not predict their occurrence, location, or magnitude. Rather, the projected increase in upper-tail burned area exceedance probabilities is consistent with broader evidence that conditions favourable to severe boreal and temperate fire seasons are expected to become more frequent under continued warming, particularly under higher-emission pathways.

The implications of this redistribution extend beyond burned area totals. A reduction in globally aggregated burned area may coexist with increasing high-impact fire activity in temperate and boreal forests, where fuel loads and biomass stocks are comparatively high. This means that global burned area decline should not be interpreted as a uniform reduction in ecological, societal, or carbon-cycle fire risk. Assessing these consequences requires additional information on fuel consumption, combustion completeness, fire severity, post-fire recovery, emissions, smoke exposure, and proximity to people and infrastructure. Nevertheless, the projected shift towards more frequent high-end burned area events in northern systems identifies these regions as a priority for further fire-risk assessment under future climate and socioeconomic pathways.

4.5 Limitations, uncertainty and future development

The reconstructions and projections should be interpreted as modelled estimates conditional on the training data and input forcing used. Although evaluation against FireCCILT11 supports the representation of large-scale spatial patterns and multi-decadal variability over 1982–2018, it cannot directly validate the early historical reconstruction or late-century projections. Uncertainty is therefore greatest outside the satellite-era evaluation period, particularly during the 1950s–1980s, when ERA5 is constrained by sparser observations than in recent decades (Hersbach et al., 2020). Observational uncertainty also affects

https://doi.org/10.5194/egusphere-2026-5374
Preprint. Discussion started: 16 September 2026

both the MODIS MCD64A1 training data, which can omit small fires and fires beneath dense vegetation or cloud cover, and the AVHRR-based FireCCILT11 evaluation product (Ramo et al., 2021; Giglio and Roy, 2022; Chen and Giglio, 2025). Performance was weakest in Deserts and Xeric Shrublands, indicating that projected changes in arid, episodic, and spatially localised fire regimes warrant particular caution.

The framework represents human influences using population density, GDP, HDI, and road length, which provide correlated proxies for human presence, access, development, land management, ignition opportunity, and potential suppression capacity. These variables cannot resolve local fire-use practices, governance, fire-management policy, suppression resources, or cultural burning (Bowman et al., 2011; Andela et al., 2017). Modelled historical and future road networks introduce further uncertainty. Similarly, the use of a fixed contemporary biome mask means that biome-level summaries do not represent biome migration or changing biome extent (Dinerstein et al., 2017). These limitations reinforce that the model cannot attribute observed or projected changes to individual climatic, socioeconomic, or land-cover drivers.

Future estimates also remain conditional on CMIP6 climate forcing and SSP assumptions (Eyring et al., 2016; IPCC, 2021). ESM-specific model fitting can accommodate some systematic differences between ESM forcing and ERA5, but it cannot remove uncertainty in climate-model structure, regional climate biases, scenario trajectories, or future land use and management. In addition, the ~25 km monthly resolution is not intended to resolve small fires, short-lived weather extremes, topographic effects or fine-scale fragmentation. The framework does not explicitly simulate dynamic CO_2 fertilisation, nutrient constraints, fire-induced mortality and regeneration, or feedbacks between fire, vegetation, and subsequent fuel development. Priority developments include evaluation against further regional burned area and fuel datasets, improved representation of dynamic vegetation type and biome transitions, and coupling to models of fire severity, emissions, smoke exposure, and post-fire recovery for downstream applications.

5 Conclusions

Sparky-Climate provides a spatially explicit, scenario-consistent reconstruction and projections of monthly global fuel characteristics and burned area at approximately 25 km resolution from 1950 to 2100. The framework harmonises historical reanalysis-driven reconstruction with CMIP6- and SSP-driven future simulations, while explicitly representing eight fuel characteristics and a broad set of meteorological, land-cover, and socioeconomic predictors. Evaluation against the observationally independent FireCCILT11 product indicates that the framework reproduces the first-order spatial, seasonal, interannual, and multi-decadal characteristics of global burned area, while also identifying limitations in some fire regimes.

The projections indicate that a declining global burned-area total does not imply a uniform reduction in fire activity or fire risk. Declining burned area in Tropical and Subtropical Grasslands and Savannas dominates the global response across

https://doi.org/10.5194/egusphere-2026-5374
Preprint. Discussion started: 16 September 2026

scenarios, whereas tropical forest responses are more variable and temperate and boreal forests show increasing projected mean burned area. Projected fuel changes similarly vary strongly among biomes, with increasing fuel loads in temperate and boreal systems and persistent reductions in tropical moist forests relative to 1950.

Changes in extreme burned area further emphasise this redistribution. Upper-tail burned-area exceedances generally decline in tropical and savanna systems but increase in temperate and boreal forests, particularly under higher-emission pathways. The framework provides a consistent basis for examining how climate, fuel conditions, land cover, and socioeconomic pathways may jointly shape future fire regimes. These estimates should be interpreted as scenario-based model projections, rather than causal attribution to individual drivers or predictions of specific future fire events.

These biome-scale shifts may also have important carbon-cycle and societal implications (Jones et al., 2024b). Increasing burned area and more frequent upper-tail events in temperate and boreal forests could have consequences disproportionate to their contribution to global burned area because these systems contain comparatively high biomass stocks. However, determining the resulting effects on emissions, radiative forcing, and carbon recovery requires explicit representation of fuel consumption, combustion completeness, fire severity, and post-fire vegetation dynamics. The harmonised dataset can also be combined with spatial projections of population, urbanisation, infrastructure, and exposure to assess potential changes in fire risk at the wildland–urban interface.

https://doi.org/10.5194/egusphere-2026-5374
Preprint. Discussion started: 16 September 2026

Table 1. Variables used to train the fuel and burned area models. Variables are derived from either historical or projected datasets and are used in one or both model frameworks. An asterisk (*) denotes variables that are modelled from the previous timestep.

Variable	Model	Historic Source	Reference	Projected	Source
High Vegetation Cover	Fuel, Burned Area	CERISE	(Tourigny et al., 2025)	LUH2	(Hurtt et al., 2020)
Low Vegetation Cover	Fuel, Burned Area	CERISE	(Tourigny et al., 2025)	LUH2	(Hurtt et al., 2020)
Type of High Vegetation	Fuel, Burned Area	CERISE	(Tourigny et al., 2025)	LUH2	(Hurtt et al., 2020)
Type of Low Vegetation	Fuel, Burned Area	CERISE	(Tourigny et al., 2025)	LUH2	(Hurtt et al., 2020)
High Vegetation LAI	Fuel*, Burned Area	Modelled	This study	Modelled	This study
Low Vegetation LAI	Fuel*, Burned Area	Modelled	This study	Modelled	This study
Dead Foliage Load	Fuel*, Burned Area	Modelled	This study	Modelled	This study
Dead Wood Load	Fuel*, Burned Area	Modelled	This study	Modelled	This study
Live Leaf Load	Fuel*, Burned Area	Modelled	This study	Modelled	This study
Live Wood Load	Fuel*, Burned Area	Modelled	This study	Modelled	This study
Dead Foliage Moisture	Fuel*, Burned Area	Modelled	This study	Modelled	This study
Dead Wood Moisture	Fuel*, Burned Area	Sparky-Fuel	This study	Modelled	This study
Live Fuel Moisture	Fuel*, Burned Area	Sparky-Fuel	This study	Modelled	This study
Soil Moisture	Fuel, Burned Area	ERA5	(Hersbach et al., 2020)	CMIP6	(Eyring et al., 2016)
2m Temperature	Fuel, Burned Area	ERA5	(Hersbach et al., 2020)	CMIP6	(Eyring et al., 2016)
Shortwave Radiation	Fuel, Burned Area	ERA5	(Hersbach et al., 2020)	CMIP6	(Eyring et al., 2016)
Wind Speed	Fuel, Burned Area	ERA5	(Hersbach et al., 2020)	CMIP6	(Eyring et al., 2016)
Relative Humidity	Fuel, Burned Area	ERA5	(Hersbach et al., 2020)	CMIP6	(Eyring et al., 2016)
Surface Pressure	Fuel, Burned Area	ERA5	(Hersbach et al., 2020)	CMIP6	(Eyring et al., 2016)
Total Precipitation	Fuel, Burned Area	ERA5	(Hersbach et al., 2020)	CMIP6	(Eyring et al., 2016)
Precipitation 5th Percentile	Fuel, Burned Area	ERA5	(Hersbach et al., 2020)	ERA5	(Hersbach et al., 2020)
Precipitation 95th Percentile	Fuel, Burned Area	ERA5	(Hersbach et al., 2020)	ERA5	(Hersbach et al., 2020)
Temperature 5th Percentile	Fuel, Burned Area	ERA5	(Hersbach et al., 2020)	ERA5	(Hersbach et al., 2020)
Temperature 95th Percentile	Fuel, Burned Area	ERA5	(Hersbach et al., 2020)	ERA5	(Hersbach et al., 2020)
Month	Fuel	-	-	-	-
Latitude	Fuel	-	-	-	-
Longitude	Fuel	-	-	-	-
Orography	Burned Area	ECLand	(Boussetta et al., 2021)	ECLand	(Boussetta et al., 2021)
Population Density	Burned Area	Reported/Modelled	(Zhuang et al., 2024)	Modelled	(Zhuang et al., 2024)
Gross Domestic Product	Burned Area	Reported/Modelled	(Feenstra et al., 2015; Kummu et al., 2025)	Modelled	(Wang and Sun, 2022)
Human Development Index	Burned Area	Reported/Modelled	(Liu et al., 2024)	Modelled	(Liu et al., 2024)
Road Density	Burned Area	Modelled	(Meijer et al., 2018)	Modelled	This study

750

https://doi.org/10.5194/egusphere-2026-5374
Preprint. Discussion started: 16 September 2026

Table 2. Projected annual mean burned area globally and by biome for different time periods, together with the corresponding trends over each period. The table also reports the interannual standard deviation and values for all six SSP scenarios considered. The final column shows the relative change in burned area between the 2020s and 2090s for each biome and scenario.

	2020s	2045-2054	2045-2054 Trend	2070s	2070s Trend	2090s	2090s Trend	Shift 2020s-2090s (%)
Global								
SSP1-1.9	360.7 ± 50.0	297.5 ± 39.9	-0.08 ± 0.48	286.7 ± 38.7	-0.63 ± 0.25	281.5 ± 43.8	-0.72 ± 1.51	**-21.9**
SSP1-2.6	342.8 ± 34.6	287.1 ± 30.3	-0.18 ± 0.90	273.6 ± 28.4	-0.23 ± 0.51	269.2 ± 29.1	-0.81 ± 1.05	**-21.5**
SSP2-4.5	347.7 ± 32.1	308.8 ± 29.0	-1.53 ± 0.57	285.1 ± 26.6	-1.06 ± 1.02	277.4 ± 25.2	-0.38 ± 0.50	**-20.2**
SSP3-7.0	352.2 ± 33.9	328.7 ± 30.0	-0.47 ± 1.29	321.6 ± 28.9	0.16 ± 0.72	328.4 ± 29.8	-0.07 ± 0.51	**-6.7**
SSP4-3.4	361.8 ± 52.9	330.9 ± 41.3	-1.43 ± 0.62	315.3 ± 42.2	0.47 ± 0.47	314.8 ± 43.2	0.11 ± 0.56	**-13.0**
SSP5-8.5	342.8 ± 32.2	293.6 ± 26.0	-0.58 ± 0.83	292.1 ± 24.1	0.34 ± 0.51	296.5 ± 26.9	0.92 ± 0.95	**-13.5**
Non-Forest								
Tropical & Subtropical Grasslands & Savannas								
SSP1-1.9	225.9 ± 22.2	169.4 ± 14.2	-0.04 ± 0.32	159.8 ± 12.5	-0.53 ± 0.1	155.1 ± 16.3	-0.66 ± 1.22	**-31.3**
SSP1-2.6	215.6 ± 17.4	165.3 ± 14.0	-0.23 ± 0.63	153.4 ± 12.9	-0.24 ± 0.42	148.7 ± 13.5	-0.68 ± 0.84	**-31**
SSP2-4.5	219.5 ± 16.0	183.0 ± 13.9	-1.48 ± 0.5	160.2 ± 12.6	-0.91 ± 0.78	153.0 ± 11.9	-0.31 ± 0.41	**-30.3**
SSP3-7.0	223.0 ± 15.4	199.4 ± 13.3	-0.68 ± 1.14	189.0 ± 12.8	-0.03 ± 0.65	189.2 ± 14.0	-0.37 ± 0.34	**-15.2**
SSP4-3.4	227.0 ± 18.8	199.1 ± 10.6	-1.39 ± 0.42	182.2 ± 11.2	0.26 ± 0.28	179.4 ± 11.7	-0.0 ± 0.39	**-21**
SSP5-8.5	217.1 ± 16.6	168.6 ± 11.3	-0.7 ± 0.6	161.0 ± 11.7	0.06 ± 0.38	158.1 ± 13.7	0.32 ± 0.61	**-27.1**
Deserts & Xeric Shrublands								
SSP1-1.9	31.0 ± 8.7	30.5 ± 8.5	0.09 ± 0.08	30.4 ± 8.5	-0.05 ± 0.15	30.6 ± 8.8	0.05 ± 0.14	-1.2
SSP1-2.6	29.6 ± 5.7	29.3 ± 5.4	0.05 ± 0.11	29.1 ± 5.4	0.01 ± 0.05	29.0 ± 5.3	-0.05 ± 0.09	-1.9
SSP2-4.5	29.5 ± 5.3	29.2 ± 4.9	0.02 ± 0.07	29.6 ± 4.9	-0.01 ± 0.11	29.6 ± 4.7	-0.04 ± 0.11	0.2
SSP3-7.0	29.2 ± 5.9	29.2 ± 5.4	0.05 ± 0.09	29.7 ± 5.2	0.03 ± 0.08	30.3 ± 5.1	0.02 ± 0.11	3.8
SSP4-3.4	30.6 ± 10.0	30.1 ± 9.5	0.11 ± 0.1	30.5 ± 9.4	0.06 ± 0.08	30.6 ± 9.6	0.02 ± 0.14	0.3
SSP5-8.5	29.1 ± 5.1	29.3 ± 4.9	0.04 ± 0.09	30.0 ± 4.7	0.02 ± 0.08	31.0 ± 4.4	0.09 ± 0.12	**6.6**
Temperate Grasslands & Savannas								
SSP1-1.9	11.5 ± 4.6	11.6 ± 4.5	-0.02 ± 0.04	11.7 ± 4.7	-0.01 ± 0.02	11.6 ± 4.5	0.01 ± 0.02	1.1
SSP1-2.6	11.6 ± 3.1	11.9 ± 3.2	0.01 ± 0.07	12.0 ± 3.2	-0.0 ± 0.04	12.1 ± 3.2	-0.02 ± 0.04	4
SSP2-4.5	11.4 ± 2.9	11.8 ± 3.1	0.0 ± 0.05	11.9 ± 3.0	0.01 ± 0.04	12.2 ± 3.0	-0.02 ± 0.04	**7.1**
SSP3-7.0	11.4 ± 3.2	11.7 ± 3.2	0.04 ± 0.05	12.1 ± 3.3	0.02 ± 0.05	12.5 ± 3.4	0.03 ± 0.04	**10.1**
SSP4-3.4	11.6 ± 5.1	11.9 ± 5.3	0.02 ± 0.01	12.0 ± 5.5	0.06 ± 0.11	12.4 ± 5.7	0.03 ± 0.07	**6.9**
SSP5-8.5	11.2 ± 3.1	11.7 ± 3.2	0.02 ± 0.05	12.4 ± 3.2	0.03 ± 0.06	12.8 ± 3.2	0.02 ± 0.04	**14.4**
Flooded Grasslands & Savannas								
SSP1-1.9	11.5 ± 0.6	8.4 ± 0.4	0.01 ± 0.03	8.1 ± 0.3	0.0 ± 0.03	7.6 ± 0.3	-0.03 ± 0.05	**-33.8**
SSP1-2.6	11.2 ± 0.5	8.2 ± 0.7	-0.0 ± 0.08	7.9 ± 0.6	0.0 ± 0.04	7.5 ± 0.5	-0.02 ± 0.04	**-33**
SSP2-4.5	11.9 ± 0.5	9.1 ± 0.5	-0.06 ± 0.05	8.0 ± 0.6	-0.03 ± 0.04	7.8 ± 0.6	-0.01 ± 0.04	**-34.2**
SSP3-7.0	12.4 ± 0.5	10.5 ± 0.5	-0.05 ± 0.11	9.6 ± 0.6	-0.01 ± 0.05	9.5 ± 0.6	-0.04 ± 0.04	**-23.8**
SSP4-3.4	12.6 ± 0.7	10.6 ± 0.2	-0.03 ± 0.05	9.5 ± 0.4	-0.0 ± 0.08	9.2 ± 0.4	0.0 ± 0.05	**-26.6**
SSP5-8.5	11.0 ± 0.4	8.4 ± 0.7	-0.04 ± 0.05	8.1 ± 0.6	-0.03 ± 0.03	7.8 ± 0.7	0.02 ± 0.05	**-29.4**
Forest								
Tropical & Subtropical Moist Broadleaf Forests								
SSP1-1.9	31.2 ± 5.0	29.0 ± 3.9	-0.1 ± 0.1	28.6 ± 4.1	-0.04 ± 0.12	28.7 ± 4.6	-0.03 ± 0.16	**-8.1**
SSP1-2.6	28.9 ± 3.5	27.1 ± 3.2	0.02 ± 0.15	26.4 ± 2.9	-0.01 ± 0.09	26.7 ± 3.0	-0.01 ± 0.11	**-7.6**
SSP2-4.5	29.7 ± 3.5	29.9 ± 3.1	-0.04 ± 0.09	29.1 ± 3.0	-0.08 ± 0.13	28.5 ± 3.0	-0.01 ± 0.08	-4
SSP3-7.0	29.9 ± 3.5	31.0 ± 3.2	0.11 ± 0.1	33.6 ± 3.9	0.12 ± 0.14	37.2 ± 6.5	0.21 ± 0.21	**24.4**

https://doi.org/10.5194/egusphere-2026-5374
Preprint. Discussion started: 16 September 2026

SSP4-3.4	30.5 ± 4.9	30.0 ± 3.3	-0.04 ± 0.12	31.7 ± 2.7	0.07 ± 0.12	32.8 ± 2.3	0.03 ± 0.03	**7.6**
SSP5-8.5	29.5 ± 3.5	29.7 ± 3.1	0.06 ± 0.18	32.4 ± 4.0	0.13 ± 0.14	35.5 ± 6.4	0.27 ± 0.27	**20.5**
Tropical & Subtropical Dry Broadleaf Forests								
SSP1-1.9	11.3 ± 2.4	10.7 ± 2.1	-0.03 ± 0.06	10.6 ± 2.2	-0.01 ± 0.06	10.6 ± 2.3	-0.01 ± 0.09	**-5.8**
SSP1-2.6	10.7 ± 1.6	10.3 ± 1.6	0.01 ± 0.05	10.1 ± 1.4	0.01 ± 0.05	10.2 ± 1.4	0.01 ± 0.07	-5
SSP2-4.5	10.7 ± 1.5	10.5 ± 1.3	-0.01 ± 0.04	10.6 ± 1.4	-0.02 ± 0.08	10.6 ± 1.3	-0.0 ± 0.06	-0.9
SSP3-7.0	10.7 ± 1.6	10.6 ± 1.3	0.03 ± 0.06	10.7 ± 1.2	0.0 ± 0.06	11.2 ± 1.5	0.03 ± 0.05	5
SSP4-3.4	11.2 ± 2.8	10.8 ± 2.2	-0.05 ± 0.07	10.8 ± 2.3	-0.0 ± 0.08	11.0 ± 2.2	0.01 ± 0.04	-1.9
SSP5-8.5	10.5 ± 1.5	10.5 ± 1.3	0.0 ± 0.07	11.3 ± 1.3	0.03 ± 0.07	12.4 ± 1.8	0.07 ± 0.08	**17.9**
Temperate Broadleaf Forests								
SSP1-1.9	10.6 ± 3.2	10.8 ± 3.3	-0.0 ± 0.04	10.8 ± 3.2	-0.01 ± 0.03	10.7 ± 3.1	0.01 ± 0.04	1.2
SSP1-2.6	10.2 ± 2.3	10.2 ± 2.3	-0.01 ± 0.06	10.4 ± 2.3	-0.0 ± 0.05	10.5 ± 2.4	-0.02 ± 0.04	3.7
SSP2-4.5	10.1 ± 2.1	10.3 ± 2.2	0.01 ± 0.03	10.5 ± 2.2	-0.01 ± 0.03	10.7 ± 2.3	0.01 ± 0.03	**5.8**
SSP3-7.0	10.1 ± 2.4	10.5 ± 2.5	-0.0 ± 0.02	10.7 ± 2.4	0.0 ± 0.04	11.2 ± 2.6	0.01 ± 0.05	**10**
SSP4-3.4	10.4 ± 3.8	10.6 ± 3.7	0.01 ± 0.05	10.6 ± 3.7	-0.0 ± 0.02	11.1 ± 3.9	0.03 ± 0.04	**6.4**
SSP5-8.5	9.9 ± 2.3	10.4 ± 2.4	0.01 ± 0.05	11.0 ± 2.4	0.03 ± 0.05	11.5 ± 2.3	0.05 ± 0.05	**16.2**
Boreal Forests								
SSP1-1.9	9.1 ± 3.7	9.4 ± 3.7	0.04 ± 0.04	9.5 ± 3.7	0.04 ± 0.04	9.4 ± 3.7	-0.03 ± 0.1	3.8
SSP1-2.6	7.9 ± 2.8	8.3 ± 2.8	-0.0 ± 0.05	8.2 ± 2.8	0.01 ± 0.04	8.4 ± 2.8	-0.02 ± 0.06	**7.1**
SSP2-4.5	7.6 ± 2.6	8.2 ± 2.7	0.0 ± 0.05	8.3 ± 2.7	0.01 ± 0.04	8.5 ± 2.7	0.01 ± 0.03	**11.1**
SSP3-7.0	7.8 ± 2.9	8.3 ± 2.9	0.03 ± 0.05	8.5 ± 2.8	0.03 ± 0.05	8.9 ± 2.9	0.02 ± 0.04	**13.7**
SSP4-3.4	8.9 ± 4.2	9.2 ± 4.1	-0.03 ± 0.05	9.4 ± 4.2	0.02 ± 0.05	9.5 ± 4.0	-0.02 ± 0.05	**6.3**
SSP5-8.5	7.6 ± 2.6	8.2 ± 2.6	0.02 ± 0.05	8.6 ± 2.5	0.02 ± 0.05	9.0 ± 2.4	0.0 ± 0.04	**18.2**

https://doi.org/10.5194/egusphere-2026-5374
Preprint. Discussion started: 16 September 2026

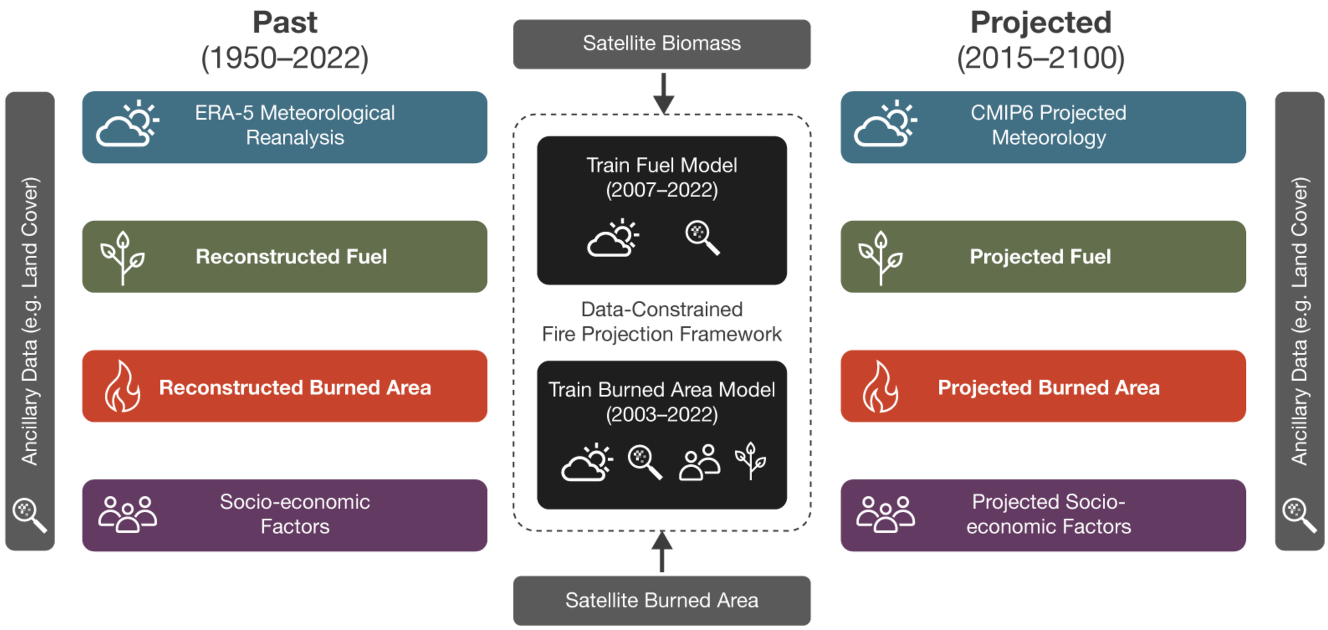

Figure 1. Schematic of the Sparky modelling framework. Historical (1950–2022) and projected (2015–2100) meteorological (blue), ancillary (grey) and socioeconomic (purple) input datasets are shown in the left and right panels, respectively. Satellite-derived biomass and burned area observations from 2015–2022 are used to train the fuel and burned area models in the central panel. The fuel model uses meteorological and ancillary inputs, whereas the burned area model uses the same variables, as well as socioeconomic inputs and the fuel model output.

https://doi.org/10.5194/egusphere-2026-5374
Preprint. Discussion started: 16 September 2026

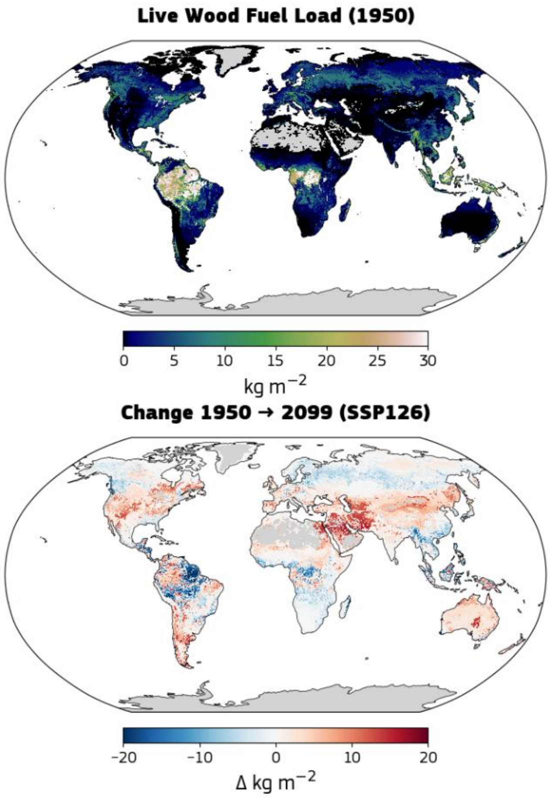

Figure 2. Global annual maps of Sparky live wood fuel load as area density (kg m⁻²) for 1950 (top left). Shifts in live fuel load from 1950 to 2020 (top right) and from 1950 to 2099 under SSP1–2.6 (bottom left) and SSP5–8.5 (bottom right).

https://doi.org/10.5194/egusphere-2026-5374
Preprint. Discussion started: 16 September 2026

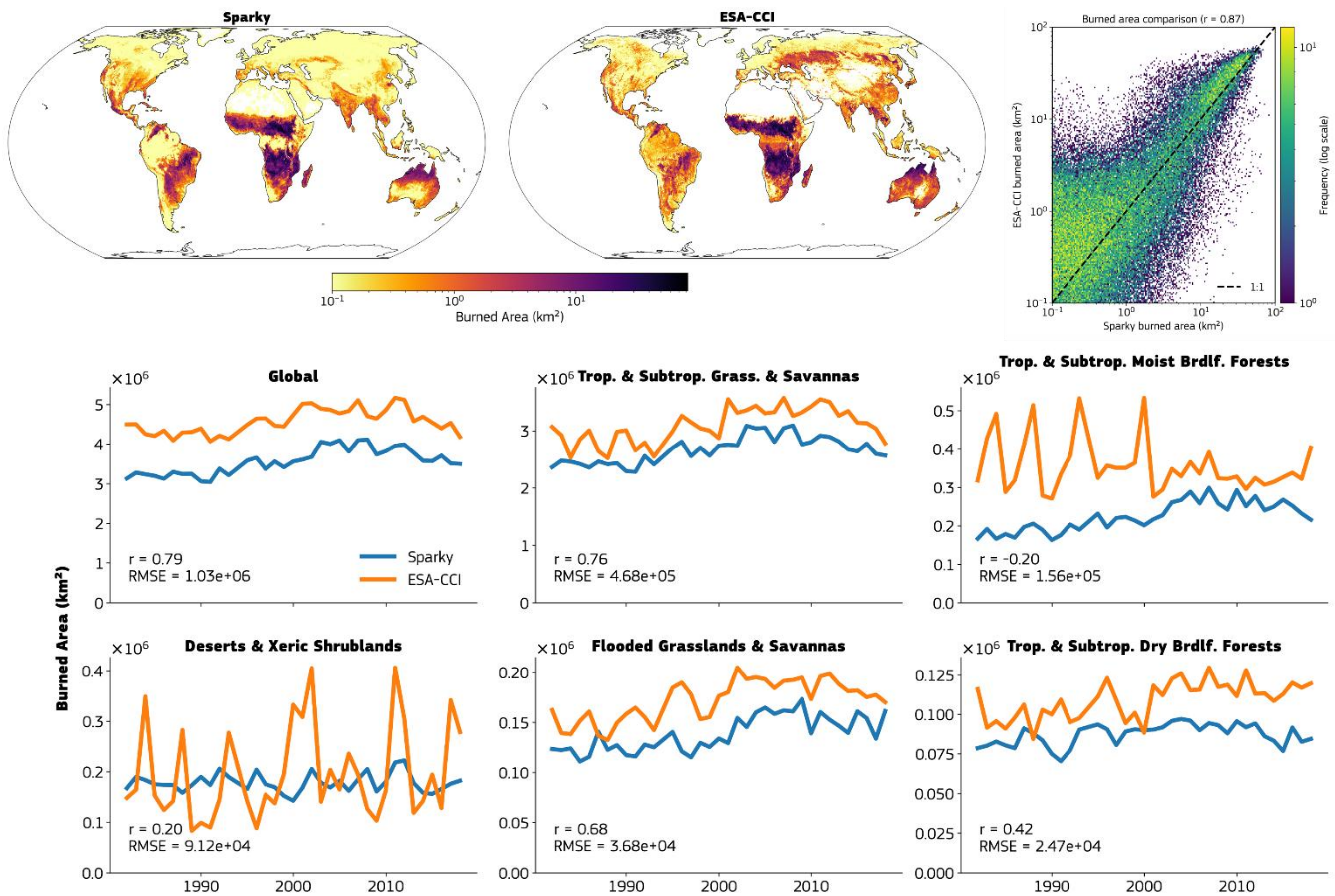

770 **Figure 3. Mean annual global burned area from 1982-2018 from Sparky model output (top left) and ESA-CCI FireCCILT11 (top middle). A two-dimensional histogram, using points and times, of Sparky burned area against ESA-CCI is shown in the top right, with the correlation coefficient. Global and biome integrated annual burned area timeseries from Sparky (blue) and ESA-CCI (orange) are shown on the bottom two rows, with correlation coefficients and Root Mean Square Errors (RMSE) indicated.**

https://doi.org/10.5194/egusphere-2026-5374
Preprint. Discussion started: 16 September 2026

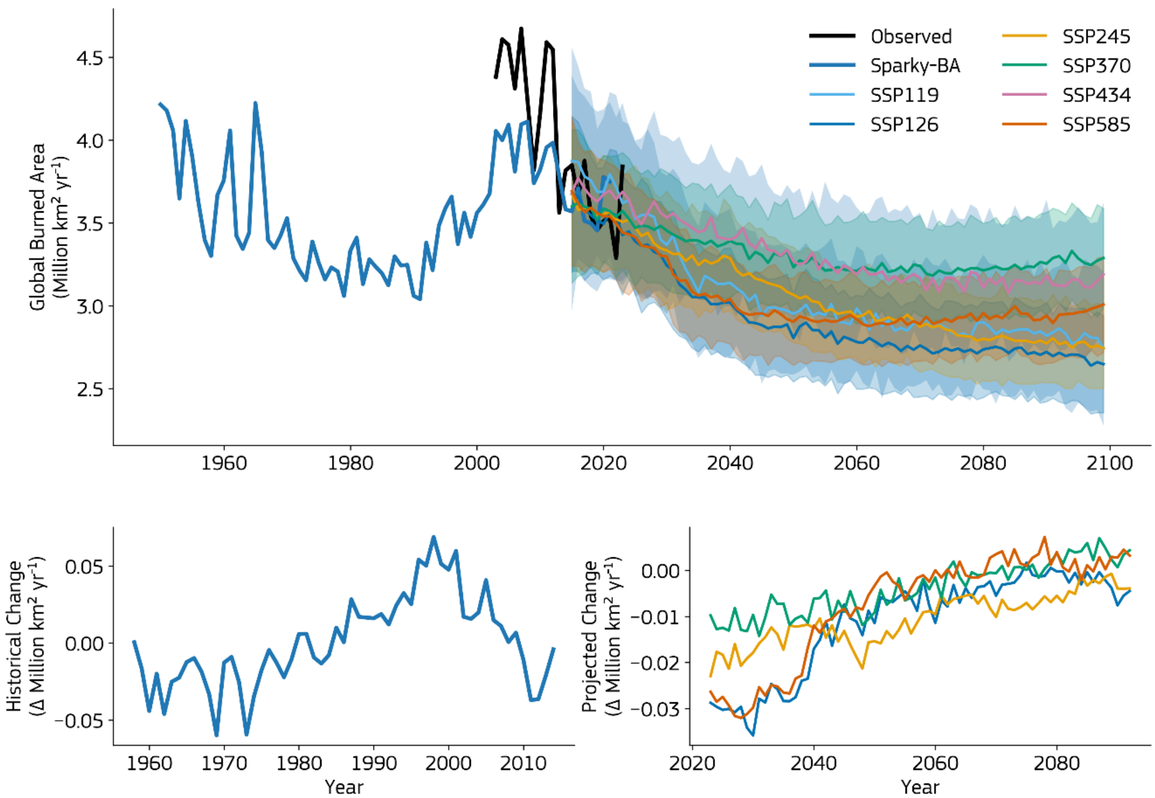

775 **Figure 4. Global annual total burned area from 1950–2100 simulated by Sparky. The historical simulation (blue) transitions into six Sparky SSP scenarios, with an overlap period from 2015–2022. The shaded area denotes the spread across CMIP6 models. MODIS-observed burned area is shown in black. The lower panels show (left) the historic global trend using a 10-year running mean and (right) projected global trends under the six SSP scenarios.**

https://doi.org/10.5194/egusphere-2026-5374
Preprint. Discussion started: 16 September 2026

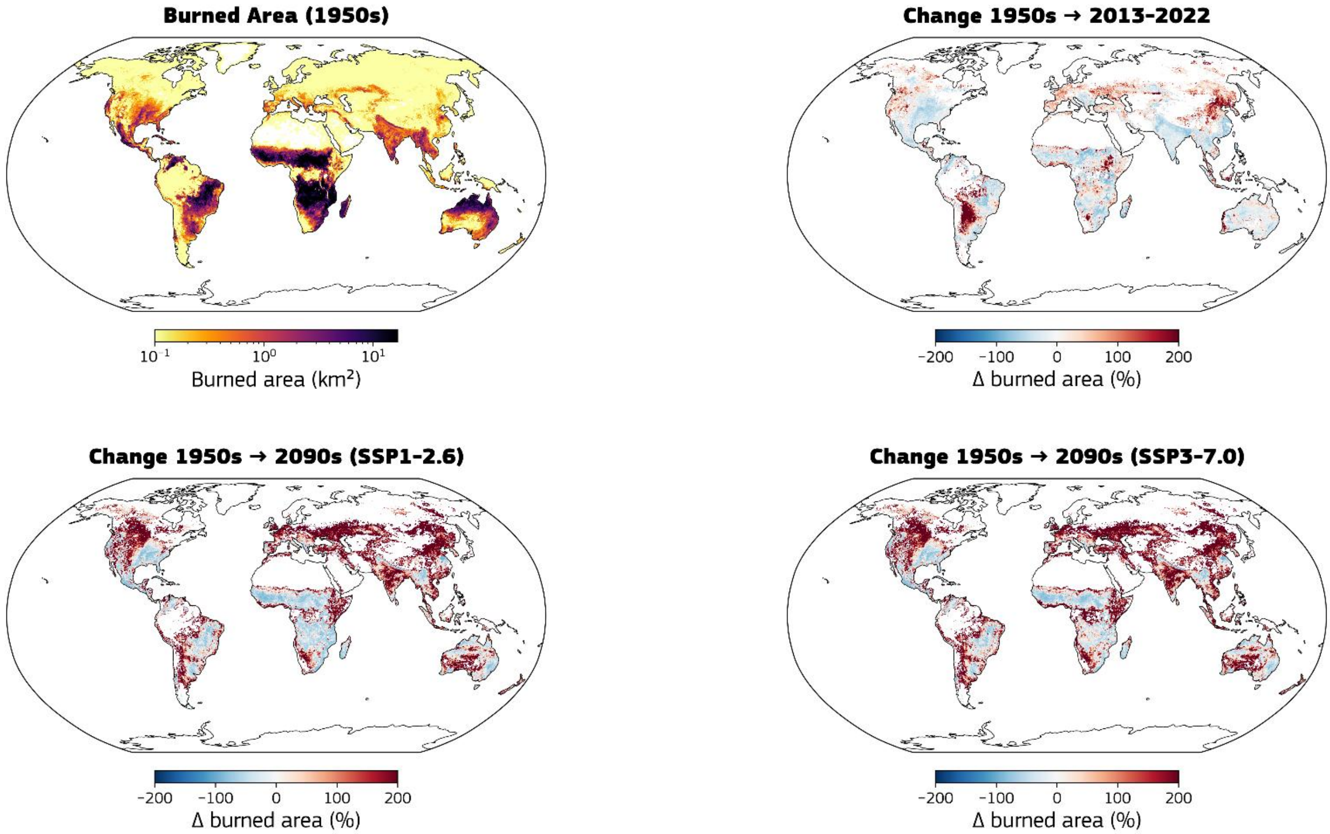

780 **Figure 5. Global annual mean maps of Sparky burned area for the 1950s (top left). Changes in mean burned area between the 1950s and 2013–2022 (top right), and between the 1950s and the 2090s under SSP1–2.6 (bottom left) and SSP3–7.0 (bottom right).**

https://doi.org/10.5194/egusphere-2026-5374
Preprint. Discussion started: 16 September 2026

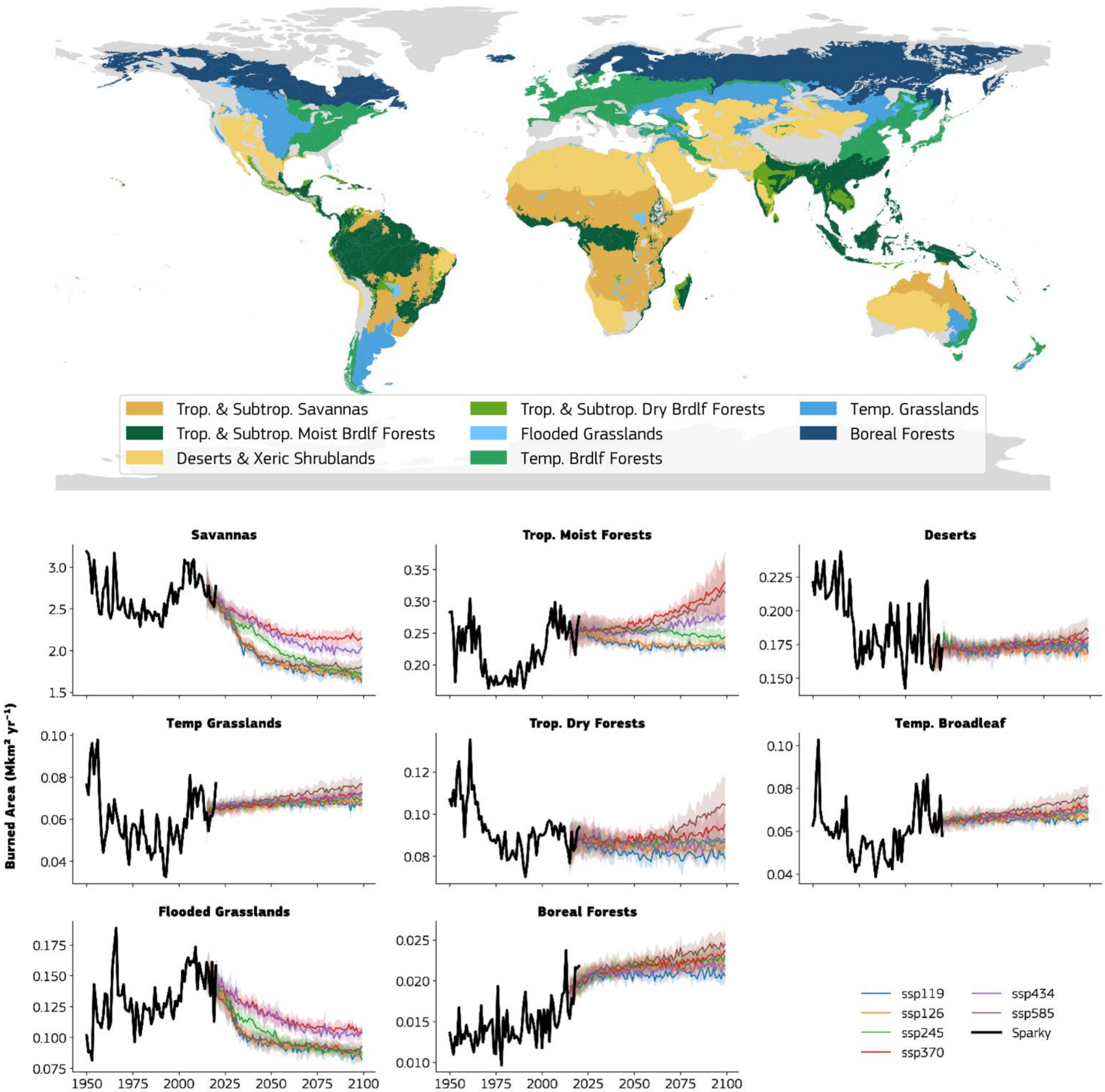

785 **Figure 6. Contemporary spatial distribution of the eight major fire biomes considered in this study(Dinerstein et al., 2017). Historical biome-specific annual total burned area from 1950–2022 simulated by Sparky (black). Projected biome-specific Sparky burned area under the six SSP scenarios from 2015–2100, with shading indicating the spread across CMIP6 models.**

https://doi.org/10.5194/egusphere-2026-5374
Preprint. Discussion started: 16 September 2026

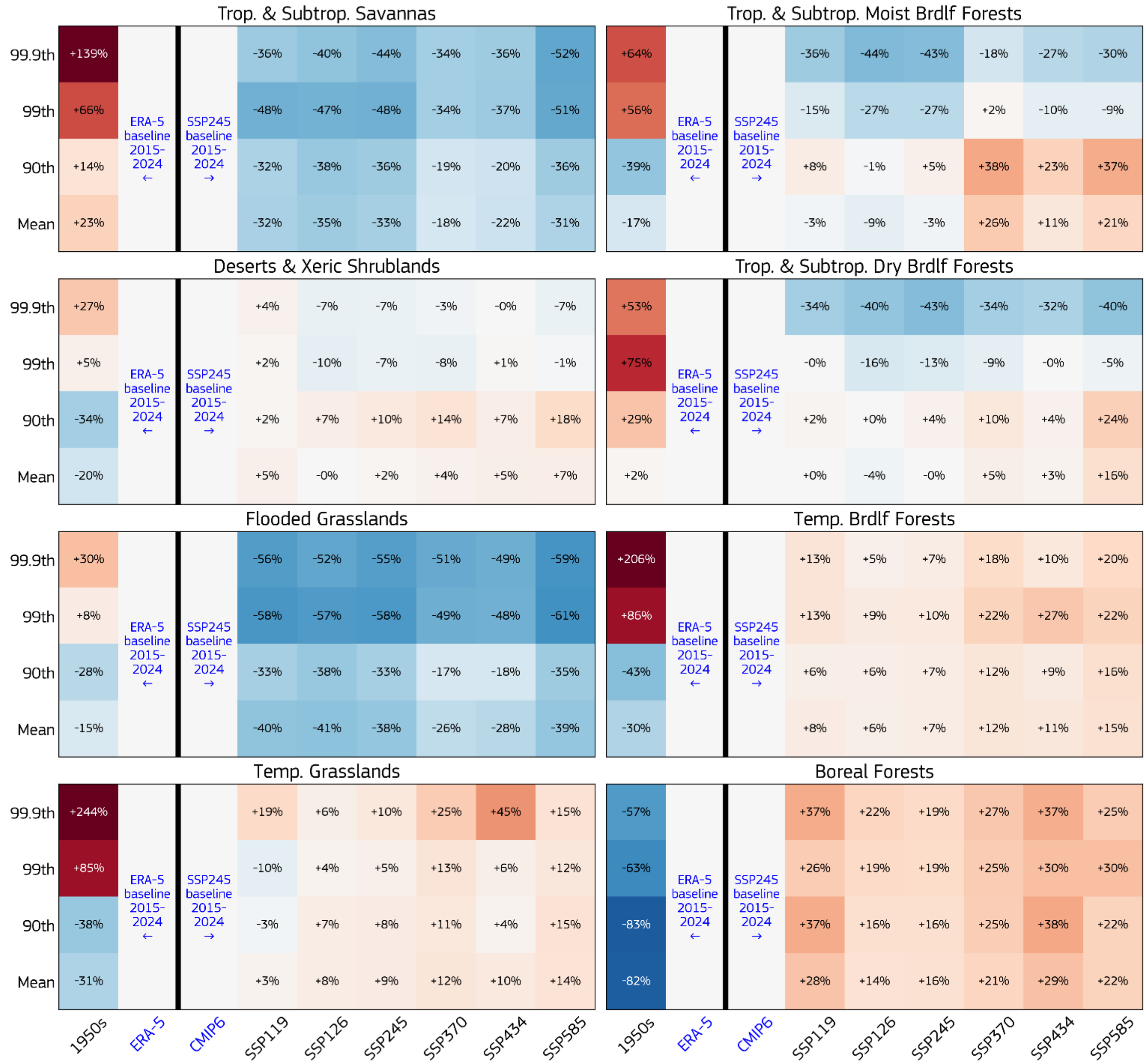

Figure 7. Changes in the probability of extreme burned-area occurrence across eight major fire biomes. Rows show thresholds corresponding to the 90th, 95th, 99th, and 99.9th percentiles of monthly grid-cell burned area during 2015–2024. Columns show probability ratios for the 1950s relative to the ERA5-driven 2015–2024 period (1st column), and for 2090–2099 SSP projections relative to the CMIP6 2015–2024 baseline (4th-9th column). Values are expressed as percentage changes in exceedance probability, with colours showing the underlying probability ratio.

https://doi.org/10.5194/egusphere-2026-5374
Preprint. Discussion started: 16 September 2026

Code and Data Availability

The Sparky-Climate burned area and fuel characteristics dataset covering 1950–2100 is available through the ECMWF Cross Data Store at: https://xds.ecmwf.int/datasets/projections-fire-fuel-burned-area (https://doi.org/10.24381/07c7cb12). The dataset includes historical reconstructions for 1950–2022, future projections for 2015–2100 under six Shared Socioeconomic Pathway (SSP) scenarios, and the associated fuel-characteristic variables used to generate the burned-area estimates.

The Sparky-Climate model is implemented in Python and relies entirely on freely available open-source software. The machine learning components are based on the XGBoost library, which provides the gradient-boosted decision tree framework used for model training and inference. All additional preprocessing, training, and analysis scripts are implemented using standard scientific Python packages.

Climate forcing data from the CMIP6 ensemble were obtained from the Earth System Grid Federation (ESGF) and accessed via the Rook Web Processing Service (WPS). Historical reanalysis data and ancillary inputs were retrieved following the access procedures described in the CDS dataset documentation (CDS; CMIP6 climate projections, 2026; https://doi.org/10.24381/cds.c866074c).

The Sparky model code and associated processing workflows are not currently distributed as a standalone software package but are fully reproducible using the described open-source dependencies and data access routes.

Supplement

The link to the supplement will be included by Copernicus.

Author Contributions

JM, ECP, FDG and CC conceptualised the study. Data curation was done by JM and ECP. The methodology was developed by JM and ECP. Analysis was done by JM. Funding acquisition was done by FDG and CC. The manuscript and visualisations were prepared by JM with review and editing support from all co-authors. Deployment and compilation of the data was done by CB.

https://doi.org/10.5194/egusphere-2026-5374
Preprint. Discussion started: 16 September 2026

Competing interests

The contact author has declared that none of the authors has any competing interests.

Financial Support

This work was supported by the Copernicus Emergency Management Service contract no. 942604 between the Joint Research Centre and ECMWF.

References

Abatzoglou, J. T. and Williams, A. P.: Impact of anthropogenic climate change on wildfire across western US forests, *Proc. Natl. Acad. Sci.*, 113, 11770–11775, https://doi.org/10.1073/pnas.1607171113, 2016.

Andela, N., Morton, D. C., Giglio, L., Chen, Y., van der Werf, G. R., Kasibhatla, P. S., DeFries, R. S., Collatz, G. J., Hantson, S., Kloster, S., Bachelet, D., Forrest, M., Lasslop, G., Li, F., Mangeon, S., Melton, J. R., Yue, C., and Randerson, J. T.: A human-driven decline in global burned area, *Science*, 356, 1356–1362, https://doi.org/10.1126/science.aal4108, 2017.

Bistinas, I., Harrison, S. P., Prentice, I. C., and Pereira, J. M. C.: Causal relationships versus emergent patterns in the global controls of fire frequency, *Biogeosciences*, 11, 5087–5101, https://doi.org/10.5194/bg-11-5087-2014, 2014.

Boussetta, S., Balsamo, G., Arduini, G., Dutra, E., McNorton, J., Choulga, M., Agustí-Panareda, A., Beljaars, A., Wedi, N., Munõz-Sabater, J., de Rosnay, P., Sandu, I., Hadade, I., Carver, G., Mazzetti, C., Prudhomme, C., Yamazaki, D., and Zsoter, E.: ECLand: The ECMWF Land Surface Modelling System, *Atmosphere*, 12, 723, https://doi.org/10.3390/atmos12060723, 2021.

Bowman, D. M. J. S., Balch, J., Artaxo, P., Bond, W. J., Cochrane, M. A., D'Antonio, C. M., DeFries, R., Johnston, F. H., Keeley, J. E., Krawchuk, M. A., Kull, C. A., Mack, M., Moritz, M. A., Pyne, S., Roos, C. I., Scott, A. C., Sodhi, N. S., and Swetnam, T. W.: The human dimension of fire regimes on Earth, *Journal of Biogeography*, 38, 2223–2236, https://doi.org/10.1111/j.1365-2699.2011.02595.x, 2011.

Chen, D. and Giglio, L.: A comprehensive assessment of the FireCCILT11 global burned area product, *Int. J. Appl. Earth Obs. Geoinf.*, 144, 104893, https://doi.org/10.1016/j.jag.2025.104893, 2025.

Chen, T. and Guestrin, C.: XGBoost: A scalable tree boosting system, in: *Proc. KDD 2016*, 785–794, https://doi.org/10.1145/2939672.2939785, 2016.

Copernicus Climate Change Service (C3S) Climate Data Store: CMIP6 climate projections (daily and monthly global climate projections from CMIP6 models), European Centre for Medium-Range Weather Forecasts (ECMWF), https://doi.org/10.24381/cds.c866074c, last access: 13 January 2026.

Copernicus Land Monitoring Service (CLMS): Leaf Area Index (LAI) 2014–present (raster 300 m), global, 10-daily, version 1, European Union's Copernicus Land Monitoring Service information, https://doi.org/10.2909/219fdc9f-616b-444b-a495-198f527b4722, last access: 3 March 2026.

https://doi.org/10.5194/egusphere-2026-5374
Preprint. Discussion started: 16 September 2026

Di Giuseppe, F., McNorton, J., Lombardi, A., and Wetterhall, F.: Global data-driven prediction of fire activity, *Nat. Commun.*, 16, 2918, https://doi.org/10.1038/s41467-025-58097-7, 2025.

Dinerstein, E., Olson, D., Joshi, A., et al.: An ecoregion-based approach to protecting half the terrestrial realm, *BioScience*, 67, 534–545, https://doi.org/10.1093/biosci/bix014, 2017.

European Centre for Medium-Range Weather Forecasts (ECMWF): Modelled Global Fuel Characteristics and Burned Area from 1950 to 2100. ECMWF Cross Data Store (XDS). Available at: https://xds.ecmwf.int/datasets/projections-fire-fuel-burned-area, last accessed: 11 August 2026.

El Garroussi, S., Di Giuseppe, F., Barnard, C., and Wetterhall, F.: Europe faces up to tenfold increase in extreme fires in a warming climate, *npj Clim. Atmos. Sci.*, 7, 30, https://doi.org/10.1038/s41612-024-00575-8, 2024.

Eyring, V., Bony, S., Meehl, G. A., Senior, C. A., Stevens, B., Stouffer, R. J., and Taylor, K. E.: Overview of the Coupled Model Intercomparison Project Phase 6 (CMIP6) experimental design and organization, *Geoscientific Model Development*, 9, 1937–1958, https://doi.org/10.5194/gmd-9-1937-2016, 2016.

Feenstra, R. C., Inklaar, R., and Timmer, M. P.: The next generation of the Penn World Table, *Am. Econ. Rev.*, 105, 3150–3182, https://doi.org/10.1257/aer.20130954, 2015.

Gallo, C., Dieppois, B., Quilcaille, Y., Chiriacò, M. V., Fulé, P. Z., Drobyshev, I., San-Miguel-Ayanz, J., Blackett, M., and Eden, J. M.: Future Impacts of Climate Change on Global Fire Weather: Insight from Weighted CMIP6 Multimodel Ensembles, *Journal of Climate*, 38, 6445–6462, https://doi.org/10.1175/JCLI-D-24-0540.1, 2025.

Giglio, L. and Roy, D. P.: Assessment of satellite orbit-drift artifacts in the long-term AVHRR FireCCILT11 global burned area data set, *Sci. Remote Sens.*, 5, 100044, https://doi.org/10.1016/j.srs.2022.100044, 2022.

Giglio, L., Boschetti, L., Roy, D. P., Humber, M. L., and Justice, C. O.: The Collection 6 MODIS burned area mapping algorithm and product, *Remote Sensing of Environment*, 217, 72–85, https://doi.org/10.1016/j.rse.2018.08.005, 2018

Guo, Z., Li, W., Ciais, P., Sitch, S., van der Werf, G. R., Bowring, S. P. K., Bastos, A., Mouillot, F., He, J., Sun, M., Zhu, L., Du, X., Wang, N., and Huang, X.: Reconstructed global monthly burned area maps from 1901 to 2020, *Earth System Science Data*, 17, 3599–3618, https://doi.org/10.5194/essd-17-3599-2025, 2025.

Hersbach, H., Bell, B., Berrisford, P., et al.: The ERA5 reanalysis, *Q. J. R. Meteorol. Soc.*, 146, 1999–2049, https://doi.org/10.1002/qj.3803, 2020.

Hubau, W., Lewis, S. L., Phillips, O. L., et al.: Asynchronous carbon sink saturation in African and Amazonian tropical forests, *Nature*, 579, 80–87, https://doi.org/10.1038/s41586-020-2035-0, 2020.

Hurtt, G. C., Chini, L., Sahajpal, R., et al.: Harmonization of global land use change and management for the period 850–2100 (LUH2) for CMIP6, *Geosci. Model Dev.*, 13, 5425–5464, https://doi.org/10.5194/gmd-13-5425-2020, 2020.

Intergovernmental Panel on Climate Change (IPCC): Climate Change 2021 – The Physical Science Basis: Working Group I Contribution to the Sixth Assessment Report of the Intergovernmental Panel on Climate Change, Cambridge University Press, Cambridge, https://doi.org/10.1017/9781009157896, 2021.

Jolly, W. M., Cochrane, M. A., Freeborn, P. H., et al.: Climate-induced variations in global wildfire danger from 1979 to 2013, *Nat. Commun.*, 6, 7537, https://doi.org/10.1038/ncomms8537, 2015.

https://doi.org/10.5194/egusphere-2026-5374
Preprint. Discussion started: 16 September 2026

Jones, M. W., Abatzoglou, J. T., Veraverbeke, S., Andela, N., Lasslop, G., Forkel, M., Smith, A. J. P., Burton, C., Betts, R. A., van der Werf, G. R., Sitch, S., Canadell, J. G., Santín, C., Kolden, C., Doerr, S. H., and Le Quéré, C.: Global and Regional Trends and Drivers of Fire Under Climate Change, *Reviews of Geophysics*, 60, e2020RG000726, https://doi.org/10.1029/2020RG000726, 2022.

Jones, M. W., Kelley, D. I., Burton, C. A., Di Giuseppe, F., Barbosa, M. L. F., Brambleby, E., Hartley, A. J., Lombardi, A., Mataveli, G., McNorton, J. R., Spuler, F. R., Wessel, J. B., Abatzoglou, J. T., Anderson, L. O., Andela, N., Archibald, S., Armenteras, D., Burke, E., Carmenta, R., Chuvieco, E., Clarke, H., Doerr, S. H., Fernandes, P. M., Giglio, L., Hamilton, D. S., Hantson, S., Harris, S., Jain, P., Kolden, C. A., Kurvits, T., Lampe, S., Meier, S., New, S., Parrington, M., Perron, M. M. G., Qu, Y., Ribeiro, N. S., Saharjo, B. H., San-Miguel-Ayanz, J., Shuman, J. K., Tanpipat, V., van der Werf, G. R., Veraverbeke, S., and Xanthopoulos, G.: State of Wildfires 2023–2024, Earth System Science Data, 16, 3601–3685, https://doi.org/10.5194/essd-16-3601-2024, 2024a.

Jones, M. W., Veraverbeke, S., Andela, N., Doerr, S. H., Kolden, C., Mataveli, G., Pettinari, M. L., Le Quéré, C., Rosan, T. M., van der Werf, G. R., van Wees, D., and Abatzoglou, J. T.: Global rise in forest fire emissions linked to climate change in the extratropics, *Science*, 386, eadl5889, https://doi.org/10.1126/science.adl5889, 2024b.

Kelley, D. I., Bistinas, I., Whitley, R., Burton, C., Marthews, T. R., and Dong, N.: How contemporary bioclimatic and human controls change global fire regimes, *Nat. Clim. Chang.*, 9, 690–696, https://doi.org/10.1038/s41558-019-0540-7, 2019.

Kim, Y.-H., Min, S.-K., Zhang, X., Sillmann, J., and Sandstad, M.: Evaluation of the CMIP6 multi-model ensemble for climate extreme indices, Weather and Climate Extremes, *Weather and Climate Extremes*, 29, 100269, https://doi.org/10.1016/j.wace.2020.100269, 2020.

Kummu, M., Kosonen, M., and Sayyar, M. M.: Downscaled gridded global dataset for gross domestic product (GDP) per capita PPP over 1990–2022, *Sci. Data*, 12, 178, https://doi.org/10.1038/s41597-025-04487-x, 2025.

Lampe, S., Gudmundsson, L., Kraft, B., Hantson, S., Kelley, D., Humphrey, V., Le Saux, B., Chuvieco, E., and Thiery, W.: BuRNN (v1.0): a data-driven fire model, *Geoscientific Model Development*, 19, 955–988, https://doi.org/10.5194/gmd-19-955-2026, 2026.

Li, F., Val Martin, M., Andreae, M. O., et al.: Historical (1700–2012) global multi-model estimates of the fire emissions from the Fire Modeling Intercomparison Project (FireMIP), *Atmos. Chem. Phys.*, 19, 12545–12567, https://doi.org/10.5194/acp-19-12545-2019, 2019.

Li, J., Miao, C., Wei, W., Zhang, G., Hua, L., Chen, Y., and Wang, X.: Evaluation of CMIP6 Global Climate Models for Simulating Land Surface Energy and Water Fluxes During 1979–2014, *Journal of Advances in Modeling Earth Systems*, 13, e2021MS002515, https://doi.org/10.1029/2021MS002515, 2021.

Liu, G., Ciais, P., Tao, S., Yang, H., Xiao, C., and Bastos, A.: A Moderate-Resolution, Long-Term Global Radar-Based Forest Above-Ground Biomass Dataset from 1993 to 2020, *Earth System Science Data Discussions*, 1–26, https://doi.org/10.5194/essd-2026-246, 2026.

Liu, K., Wang, R., Schrijver, I., and Hoekstra, R.: Can we project well-being? Towards integral well-being projections in climate models and beyond, *Humanit. Soc. Sci. Commun.*, 11, 457, https://doi.org/10.1057/s41599-024-02941-6, 2024.

McNorton, J. R. and Di Giuseppe, F.: A global fuel characteristic model and dataset for wildfire prediction, *Biogeosciences*, 21, 279–300, https://doi.org/10.5194/bg-21-279-2024, 2024.

https://doi.org/10.5194/egusphere-2026-5374
Preprint. Discussion started: 16 September 2026

McNorton, J. R., Di Giuseppe, F., Pinnington, E., Chantry, M., and Barnard, C.: A Global Probability-Of-Fire (PoF) Forecast, *Geophysical Research Letters*, 51, e2023GL107929, https://doi.org/10.1029/2023GL107929, 2024.

Meijer, J. R., Huijbregts, M. A. J., Schotten, K. C. G. J., and Schipper, A. M.: Global patterns of current and future road infrastructure, *Environ. Res. Lett.*, 13, 064006, https://doi.org/10.1088/1748-9326/aabd42, 2018.

Muñoz-Sabater, J., Dutra, E., Agustí-Panareda, A., Albergel, C., Arduini, G., Balsamo, G., Boussetta, S., Choulga, M., Harrigan, S., Hersbach, H., Martens, B., Miralles, D. G., Piles, M., Rodríguez-Fernández, N. J., Zsoter, E., Buontempo, C., and Thépaut, J.-N.: ERA5-Land: a state-of-the-art global reanalysis dataset for land applications, *Earth System Science Data*, 13, 4349–4383, https://doi.org/10.5194/essd-13-4349-2021, 2021.

O'Neill, B. C., Tebaldi, C., van Vuuren, D. P., Eyring, V., Friedlingstein, P., Hurtt, G., Knutti, R., Kriegler, E., Lamarque, J.-F., Lowe, J., Meehl, G. A., Moss, R., Riahi, K., and Sanderson, B. M.: The Scenario Model Intercomparison Project (ScenarioMIP) for CMIP6, Geoscientific Model Development, 9, 3461–3482, https://doi.org/10.5194/gmd-9-3461-2016, 2016.

Otón, G., Lizundia-Loiola, J., Pettinari, M. L., and Chuvieco, E.: Development of a consistent global long-term burned area product (1982–2018) based on AVHRR-LTDR data, *Int. J. Appl. Earth Obs. Geoinf.*, 103, 102473, https://doi.org/10.1016/j.jag.2021.102473, 2021.

Parry, I. M., Ritchie, P. D. L., and Cox, P. M.: Evidence of localised Amazon rainforest dieback in CMIP6 models, *Earth System Dynamics*, 13, 1667–1675, https://doi.org/10.5194/esd-13-1667-2022, 2022.

Perkins, O., Kasoar, M., Voulgarakis, A., Smith, C., Mistry, J., and Millington, J. D. A.: A global behavioural model of human fire use and management: WHAM! v1.0, *Geoscientific Model Development*, 17, 3993–4016, https://doi.org/10.5194/gmd-17-3993-2024, 2024.

Quilcaille, Y., Batibeniz, F., Ribeiro, A. F. S., Padrón, R. S., and Seneviratne, S. I.: Fire weather index data under historical and shared socioeconomic pathway projections in the 6th phase of the Coupled Model Intercomparison Project from 1850 to 2100, *Earth System Science Data*, 15, 2153–2177, https://doi.org/10.5194/essd-15-2153-2023, 2023.

Ramo, R., Roteta, E., Bistinas, I., van Wees, D., Bastarrika, A., Chuvieco, E., and van der Werf, G. R.: African burned area and fire carbon emissions are strongly impacted by small fires undetected by coarse resolution satellite data, *Proc. Natl. Acad. Sci.*, 118, e2011160118, https://doi.org/10.1073/pnas.2011160118, 2021.

Santoro, M., Cartus, O., Quegan, S., et al.: Design and performance of the Climate Change Initiative Biomass global retrieval algorithm, *Sci. Remote Sens.*, 10, 100169, https://doi.org/10.1016/j.srs.2024.100169, 2024.

Thorarinsdottir, T. L., Sillmann, J., Haugen, M., Gissibl, N., and Sandstad, M.: Evaluation of CMIP5 and CMIP6 simulations of historical surface air temperature extremes using proper evaluation methods, *Environ. Res. Lett.*, 15, 124041, https://doi.org/10.1088/1748-9326/abc778, 2020.

Tourigny, E., Mozaffari, A., Huggannavar, V., Ayan, I., Choulga, M., Boussetta, S., and Fairbairn, D.: Time-varying lake cover, land cover and LAI and extension of CONFESS vegetation data back to 1925 datasets, CERISE Project Deliverable D7.4, Barcelona Supercomputing Center (BSC), Copernicus Climate Change Service Evolution (CERISE) project, April 2025, available at: https://www.cerise-project.eu/sites/default/files/2025-05/CERISE-D7-4-V1.0.pdf, last access: 3 March 2026.

https://doi.org/10.5194/egusphere-2026-5374
Preprint. Discussion started: 16 September 2026

Van Wagner, C. E.: Structure of the Canadian forest fire weather index system, *Canadian Forestry Service*, Environment Canada, Forestry Technical Report 1333, Ottawa, Canada, 1974.

Wang, T. and Sun, F.: Global gridded GDP data set consistent with the shared socioeconomic pathways, *Sci. Data,* 9, 221, https://doi.org/10.1038/s41597-022-01300-x, 2022.

Wei, N. and Xia, J.: Robust projections of increasing land carbon storage in boreal and temperate forests under future climate change scenarios, *One Earth*, 7, 88–99, https://doi.org/10.1016/j.oneear.2023.11.013, 2024.

Zheng, B., Ciais, P., Chevallier, F., Chuvieco, E., Chen, Y. and Yang, H.: Increasing forest fire emissions despite the decline in global burned area. *Science advances*, *7*(39), https://doi.org/10.1126/sciadv.abh2646 , 2021.

Zhuang, H., Liu, X., Li, B., Wu, C., Yan, Y., Zeng, L., and Zheng, C.: Mapping high-resolution global gridded population distribution from 1870 to 2100, *Science of The Total Environment*, 955, 176867, https://doi.org/10.1016/j.scitotenv.2024.176867, 2024.

Appendix

Table A1. A summary of the target variables and their sources considered by both the fuel and burned area Sparky models.

Target Variable	Model	Target Source	Reference	Period
High Vegetation LAI	Fuel	CLMS LAI	(CLMS-LAI, 2025)	2015-2022
Low Vegetation LAI	Fuel	CLMS LAI	(CLMS-LAI, 2025)	2015-2022
Dead Foliage Load	Fuel	ESA-CCI / Fuel Model	(McNorton and Di Giuseppe, 2024; Santoro et al., 2024)	2015-2022
Dead Wood Load	Fuel	ESA-CCI / Fuel Model	(McNorton and Di Giuseppe, 2024; Santoro et al., 2024)	2015-2022
Live Leaf Load	Fuel	ESA-CCI / Fuel Model	(McNorton and Di Giuseppe, 2024; Santoro et al., 2024)	2015-2022
Live Wood Load	Fuel	ESA-CCI / Fuel Model	(McNorton and Di Giuseppe, 2024; Santoro et al., 2024)	2015-2022
Dead Foliage Moisture	Fuel	ERA5 / Fuel Model	(Hersbach et al., 2020; McNorton and Di Giuseppe, 2024)	2015-2022
Dead Wood Moisture	Fuel	ERA5 / Fuel Model	(Hersbach et al., 2020; McNorton and Di Giuseppe, 2024)	2015-2022
Live Fuel Moisture	Fuel	ERA5 / Fuel Model	(Hersbach et al., 2020; McNorton and Di Giuseppe, 2024)	2015-2022
Burned Area Fraction	Burned Area	MODIS C6.1	(Giglio et al., 2018)	2015-2024

https://doi.org/10.5194/egusphere-2026-5374
Preprint. Discussion started: 16 September 2026

Table A2. Summary of SSP scenarios used to generate projection based on O'Neill *et al.* (2016).

Scenario	SSP family	Narrative	Radiative forcing (W/m²)	Approx. global warming by 2100 (°C)	Description
SSP1-1.9	SSP1 - Sustainability	Taking the Green Road	1.9	~1.5	Very low emissions; consistent with the Paris Agreement 1.5 °C target
SSP1-2.6	SSP1 — Sustainability	Taking the Green Road	2.6	~1.8	Low emissions; strong mitigation and sustainable development
SSP2-4.5	SSP2 — Middle of the Road	Middle of the Road	4.5	~2.7	Intermediate emissions; social and economic trends broadly follow historical patterns
SSP3-7.0	SSP3 — Regional Rivalry	A Rocky Road	7.0	~3.6	Medium-high emissions; regional rivalry, no additional climate policy
SSP4-3.4	SSP4 — Inequality	A Road Divided	3.4	~2.4	Low-to-intermediate emissions within a world of high inequality
SSP5-8.5	SSP5 — Fossil-fueled Development	Taking the Highway	8.5	~4.4	Very high emissions; fossil-fueled development with no additional climate policy

Table A3. CMIP6 ESMs meeting variable completeness criteria and the considerations of humidity, top soil layer and SSPs used.

Model	Humidity variable	Top soil layer thickness	Scenario Considered
ACCESS-CM2	specific humidity	0.1 m	SSP1-2.6, SSP2-4.5, SSP3-7.0, SSP5-8.5
CanESM5-CanOE	relative humidity	0.1 m	SSP1-2.6, SSP2-4.5, SSP3-7.0, SSP5-8.5
CMCC-CM2-SR5	specific humidity	0.1 m	SSP1-2.6, SSP2-4.5, SSP3-7.0, SSP5-8.5

https://doi.org/10.5194/egusphere-2026-5374
Preprint. Discussion started: 16 September 2026

CMCC-ESM2	specific humidity	0.1 m	SSP1-2.6, SSP2-4.5, SSP5-8.5
CNRM-CM6-1-HR	relative humidity	0.05 m	SSP1-2.6, SSP2-4.5, SSP3-7.0, SSP5-8.5
CNRM-ESM2-1	relative humidity	0.05 m	SSP1-1.9, SSP1-2.6, SSP2-4.5, SSP3-7.0, SSP4-3.4, SSP5-8.5
E3SM-1-1	specific humidity	0.1 m	SSP5-8.5
EC-Earth3-CC	relative humidity	0.1 m	SSP2-4.5, SSP5-8.5
KACE-1-0-G	specific humidity	0.1 m	SSP2-4.5, SSP3-7.0, SSP5-8.5
MIROC6	specific humidity	0.1 m	SSP1-1.9, SSP1-2.6, SSP2-4.5, SSP3-7.0, SSP4-3.4, SSP5-8.5
MIROC-ES2L	specific humidity	0.1 m	SSP1-1.9, SSP1-2.6, SSP2-4.5, SSP3-7.0, SSP5-8.5
MPI-ESM1-2-LR	specific humidity	0.1 m	SSP1-2.6, SSP2-4.5, SSP3-7.0, SSP5-8.5
MRI-ESM2-0	specific humidity	0.1 m	SSP1-1.9, SSP1-2.6, SSP2-4.5, SSP3-7.0, SSP4-3.4, SSP5-8.5
NorESM2-MM	specific humidity	0.1 m	SSP1-2.6, SSP2-4.5, SSP3-7.0, SSP5-8.5
UKESM1-0-LL	specific humidity	0.1 m	SSP1-1.9, SSP1-2.6, SSP2-4.5, SSP3-7.0, SSP4-3.4, SSP5-8.5

Table A4. CMIP6 and ERA5 variable definitions and unit conversions applied during preprocessing.

Variable	**ERA5 units**	**CMIP6 units**	**Conversion applied**
2 m air temperature	K	K	None
Near-surface relative humidity	%	%	None
Near-surface specific humidity	kg kg^{-1}	1 (volume mixing ratio)	None
Soil moisture	m^{3} m^{-3} (Soil water volume, layer 1)	kg m^{-2} (mass of water per unit area in the uppermost soil layer)	Divide by 100 (assuming layer depth of 0.1 m)
Surface downwelling shortwave radiation	J m^{-2} day^{-1}	W m^{-2}	Multiply by 86,400 s day^{-1}
10 m wind speed	m s^{-1}	m s^{-1}	None
Surface air pressure	Pa	Pa	None
Total precipitation	m day^{-1}	kg m^{-2} s^{-1}	Multiply by 86,400 s day^{-1}, divide by 1000 kg m^{-3}

https://doi.org/10.5194/egusphere-2026-5374
Preprint. Discussion started: 16 September 2026

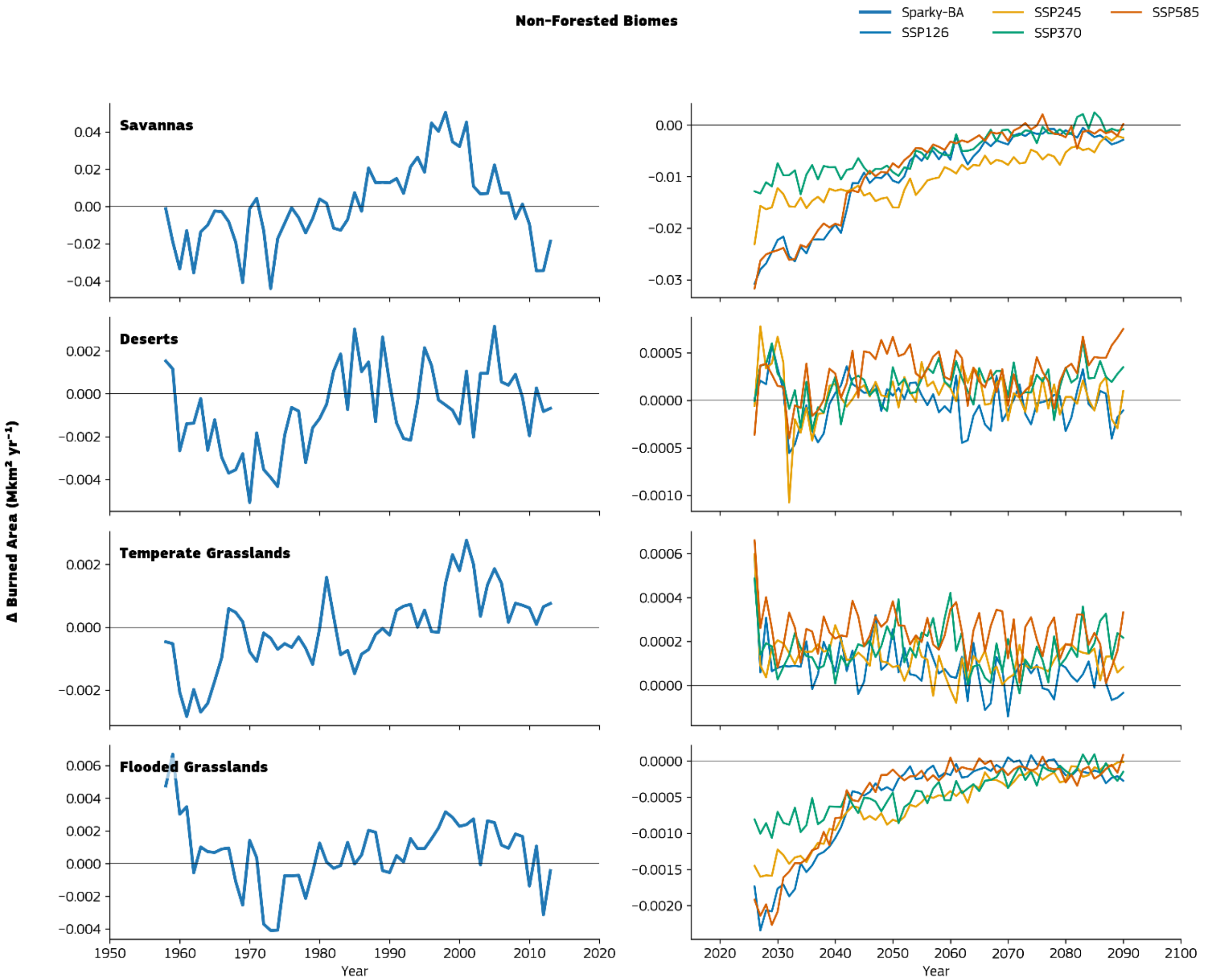

Figure A1. The left column panels show the historic non-forested biome-specific annual burned area trend using a 10-year running mean from Sparky and the right column panels show the projected trends under the six SSP scenarios.

https://doi.org/10.5194/egusphere-2026-5374
Preprint. Discussion started: 16 September 2026

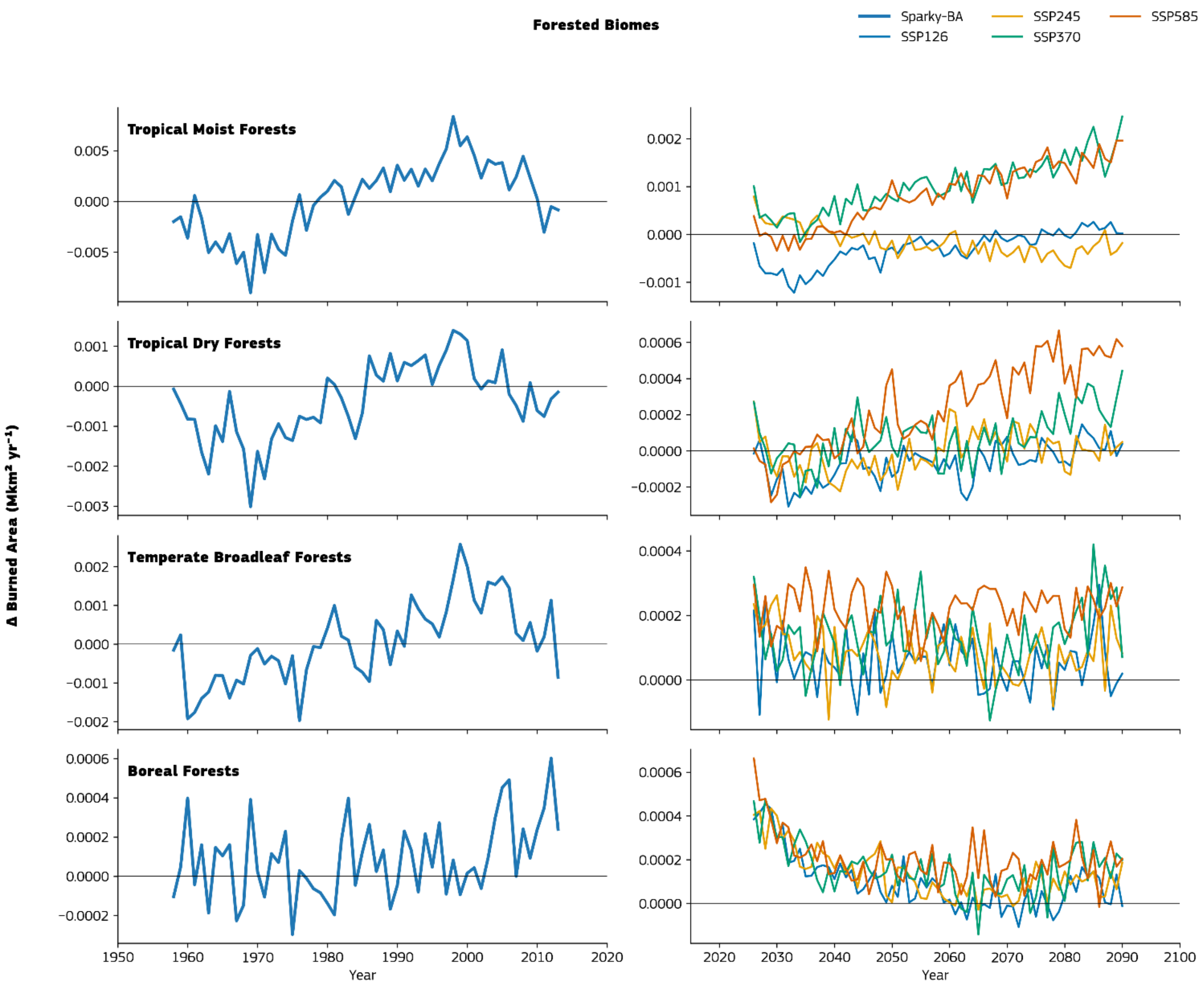

985 **Figure A2. The left column panels show the historic forested biome-specific annual burned area trend using a 10-year running mean from Sparky and the right column panels show the projected trends under the six SSP scenarios.**

https://doi.org/10.5194/egusphere-2026-5374
Preprint. Discussion started: 16 September 2026

References

Buiter, S.: How syn-rift sedimentation promotes the formation of hyper-extended margins, EGU General Assembly 2020, Online, 4–8 May 2020, EGU2020-18622, https://doi.org/10.5194/egusphere-egu2020-18622, 2020.

Loew, A., Bennartz, R., Fell, F., Lattanzio, A., Doutriaux-Boucher, M., and Schulz, J.: Surface Albedo Validation Sites, EUMETSAT [data set], https://doi.org/10.15770/EUM_SEC_CLM_1001, 2015.

Porter, J. G., De Bruyn, W., and Saltzman, E. S.: Eddy flux measurements of sulfur dioxide deposition to the sea surface, Atmos. Chem. Phys., 18, 15291–15305, https://doi.org/10.5194/acp-18-15291-2018, 2018.

Jung, M., Koirala, S., Weber, U., Ichii, K., Gans, F., Gustau-Camps-Valls, Papale, D., Schwalm, C., Tramontana, G., and Reichstein, M.: The FLUXCOM ensemble of global land-atmosphere energy fluxes, arXiv [preprint], arXiv:1812.04951, 11 December 2018.

Randall, D., Dazlich, D., Heikes, R., and Konor, C.: CSU model for DCMIP 2016, Zenodo [code], https://doi.org/10.5281/zenodo.5800992018, 2017.

Singh, O. N. and Fabian, P. (Eds.): Atmospheric Ozone: a Millennium Issue, Copernicus Publications, Katlenburg-Lindau, Germany, 147 pp., ISBN 393658608X, 2003.

van Edig, X., Schwarze, S., and Zeller, M.: The robustness of indicator based poverty assessment tools in changing environments – empirical evidence from Indonesia, in: Tropical Rainforests and Agroforests under Global Change, Environmental Science and Engineering (Environmental Engineering), edited by: Tscharntke, T., Leuschner, C., Veldkamp, E., Faust, H., Guhardja, E., and Bidin, A., Springer, Berlin, Heidelberg, Germany, 191–211, https://doi.org/10.1007/978-3-642-00493-3_9, 2010.